Mathematical Institute

UNIVERSITY OF OXFORD

Peter Julius Waldert, BSc BSc

Wolfson College

General Kernel Spectral Methods for Equilibrium Measures

MASTER'S THESIS

a thesis submitted for the degree of

Master of Science (MSc)

in

Mathematical Modelling and Scientific Computing (MMSC)

submitted to the

University of Oxford

Academic Supervisors

Dr. Timon Gutleb[a]

Prof. José A. Carrillo de la Plata MA, FEurASc, FSIAM, MAE, FIMA[a]

[a]Mathematical Institute, University of Oxford

Oxford, August 2023

Abstract

This MMSC thesis with a catchy abstract will explore general kernel spectral methods for finding equilibrium measures where initial progress was made in Gutleb, José A. Carrillo and S. Olver 2022b and Gutleb, José A. Carrillo and S. Olver 2022a.

To be done / included.

Statement of Originality: The extension of the attractive-repulsive kernel spectral method into a general kernel spectral method along with an implementation of it is original. All code contributions, starting from the particle simulation software to the implementation of the spectral methods, are entirely original.

Keywords: Pairwise Interaction Potentials, Many-Body Systems, Particle Simulations, Swarming Behaviours, Equilibrium Measures, Spectral Methods, Orthogonal Polynomials, Numerical Analysis

Languages: C++, Julia, Python

Acknowledgements

Primarily, I want to thank my supervisors Dr. Timon Gutleb and Prof. José Carillo for their valuable support in the research and writing process of this dissertation. I would also like to extend further gratitude to our course director, Dr. Kathryn Gillow, for her never-ending, reliable support to all of us throughout the course. I also want to thank my departmental and college supervisors, Prof. Yuji Nakatsukasa and Dr. Jani Bolla for their positive influence and good advice.

I would like to thank the Steirische Stipendienstiftung for their generous support which enabled me to pursue this degree in the first place.

Contents

1 Introduction **6**

1.1 Problem Setting 6

1.2 Notational Conventions 7

2 Particle Interaction Theory **9**

2.1 A Many-Body System 9

2.1.1 Attractive-Repulsive Potential 10

2.1.2 Morse Potential 10

2.2 Continuous Limit 11

2.2.1 The Problem 12

2.3 Self-Propulsion 12

2.4 Kinetic Theory: The Vlasov Equation 13

2.5 Vicsek Model 14

2.6 Swarming in Biological Settings 14

2.7 Analytical Solutions 14

3 Particle Simulator **15**

3.1 Available Methods 16

3.1.1 Leapfrog Integration 17

3.2 Phase Space 17

3.3 Runtime Analysis 19

4 Spectral Method **20**

4.1 Orthogonal Polynomials forming a Basis 20

4.2 Derivation of Operator 30

4.3 Results 32

4.4 Outer Optimisation Routine 33

4.5 Comparison with Analytic Solutions 33
4.6 Discussion 35

5 General Kernel Spectral Method 38

6 Implementation and Results 42
6.1 Further Discussion 43
6.1.1 Well-Conditionedness 43
6.2 Implementation Architecture 44
6.3 Runtime Analysis 44

7 Conclusion 45
7.1 Summary 45
7.2 Future Work 46
7.3 Conclusion 46

Acronyms, Definitions and Theorems 47

Bibliography 49

List of Figures and Tables 51

A Various Parameters 53

Chapter 1

Introduction

This chapter will give a brief overview of the setting of the problem considered in this dissertation, motivate a few biological and physical examples, and set up some notational conventions.

1.1 Problem Setting

The present thesis is concerned with many-body systems, treating particles in an abstract sense as they could take the form of physical atoms, birds in a flock or fish in a school. Other examples include ant colonies and swarms of insects such as locusts. A swarm of animals, a set of coordinated entities, brings many advantages for its members. For example, they share water resistance or it is easier to find a mate within the swarm than otherwise. They also often mimic larger animals to fend off predators and swarming behaviour ("swarm intelligence") plays an important role in this process. There are some disadvantages as well, like the accelerated spread of diseases or when resources are scarce, some swarm species even begin cannibalistic behaviour (D'Orsogna 2017).

From a more physical perspective, pair potentials $K : \mathbb{R}^+ \mapsto \mathbb{R}$ provide a simple and computationally efficient way to approximate the interaction between two particles based solely on their distance (cf. Figure 1.1a as a simple illustration). Pairwise potentials can be used to approximate a wide range of interactions, including interatomic potentials in physics and computational chemistry. Common examples of pair potentials include the Lennard-Jones potential and the Morse potential, which are widely used in molecular dynamics simulations to study the behavior of atoms and

molecules, as well as the Coulomb potential used to describe the interaction between two charges in electrodynamics.

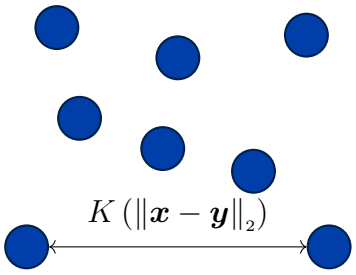

(a) $N = 8$ particles interacting with one another through the potential $K(r)$.

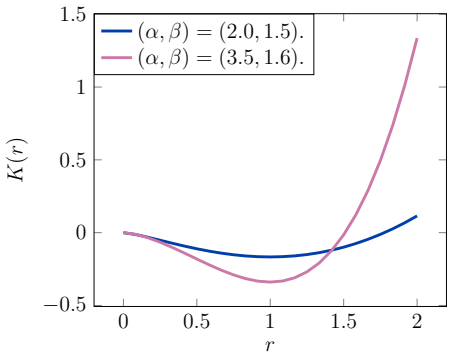

(b) Plot of attractive-repulsive potential functions $K_{\alpha,\beta}(r) = \frac{r^\alpha}{\alpha} - \frac{r^\beta}{\beta}$ for different α, β.

From here on, we will refer to said swarm entities, be it fish, birds or atoms, as *particles*.

1.2 Notational Conventions

Let $\mathbb{N}$ denote the natural numbers (positive integers) without 0 and let $\mathbb{N}_0 := \mathbb{N} \cup \{0\}$. In the following, we will use **bold** notation for vectors, matrices will generally be denoted by a capital letter and scalars by a lowercase letter. We will frequently make use of the (Euclidean) 2-norm of a vector, as denoted by $\|\cdot\|_2$. So for a d-dimensional vector $\boldsymbol{x} \in \mathbb{R}^d$ we have $\|\boldsymbol{x}\|_2 := \sqrt{\sum_{k=1}^d x_k^2}$. Also note that for readability, we will use the notation $\boldsymbol{x}^2 := \boldsymbol{x}^T\boldsymbol{x} = \|\boldsymbol{x}\|_2^2 \in \mathbb{R}^+$.

One should also clarify the nature of a few of the integrals appearing in this thesis which are often performed over the closed unit ball $B_1(\boldsymbol{x}) := \{\boldsymbol{y} \in \mathbb{R}^d \mid \|\boldsymbol{x}-\boldsymbol{y}\|_2 \leq 1\}$ centered at the origin $\boldsymbol{x} = \boldsymbol{0}$. These volume integrals (often ended by $\mathrm{d}^d y$ or $\mathrm{d}V$) over the d-dimensional unit ball shall be written as

$$\int_{B_1(\boldsymbol{0})} \mathrm{d}\boldsymbol{y}\,,$$

where $\boldsymbol{y} \in \mathbb{R}^d$ is the integration variable. Note that some definitions of $B_1(\boldsymbol{x})$ are open sets, leaving out the shell $\{\boldsymbol{y} \in \mathbb{R}^d \mid \|\boldsymbol{x}-\boldsymbol{y}\|_2 = 1\}$. The choice of definition does not matter for our purposes as the shell, a hyperplane of Lebesgue measure 0, does not contribute to the integral.

All numerical plots and figures in this thesis were generated using the Makie visualisation tool (Danisch and Krumbiegel 2021), an open-source package available for the Julia computing language (Bezanson et al. 2017).

Chapter 2

Particle Interaction Theory

As mentioned in the introduction.

2.1 A Many-Body System

is a set of particles with position and velocity interacting with one another. Each particle individually is subject to inertia and its kinetic energy ("second moment" [1]) is given by

$$E_{\text{kin},i} = \frac{\boldsymbol{p_i}^2}{2m} = \frac{(m\boldsymbol{v_i})^2}{2m} = \frac{1}{2}m \left\|\boldsymbol{v_i}\right\|_2^2 .$$

The second important ingredient is an interaction potential motivating pairwise forces $\boldsymbol{F_{ij}} \in \mathbb{R}^d$ between particles

$$\boldsymbol{F}_{ij} = -\nabla U_{ij} = -\left(\partial x_1, ..., \partial x_d\right)^T U_{ij} .$$

The total potential of a system of $N_p \geq 2$ particles $U \in \mathbb{R}$ can be calculated by summing up the pair potentials $U_{ij} \in \mathbb{R}$ between all pairs of particles

$$U = \sum_{i=1}^{N_p} \sum_{j=1, j\neq i}^{N_p} U_{ij} = \sum_{i=1}^{N_p} \sum_{j=1, j\neq i}^{N_p} K\left(\left\|\boldsymbol{x_i} - \boldsymbol{x_j}\right\|_2\right) ,$$

where $\boldsymbol{x_i} \in \mathbb{R}^d$ represents the d-dimensional position of particle i, respectively.

In the absence of an external potential V, the total energy is given by $E = E_{\text{kin}} + U$, so

$$E = \frac{1}{2}\sum_{i=1}^{N_p} m_i \boldsymbol{v_i}^2 + \sum_{i=1}^{N_p} \sum_{j=1, j\neq i}^{N_p} K\left(\left\|\boldsymbol{x_i} - \boldsymbol{x_j}\right\|_2\right) . \tag{2.1}$$

[1] In kinetic theory, the 0th moment is the mass m_i of a particle, the first moment is the momentum $\boldsymbol{p_i}$ and the second moment is its kinetic energy $E_{kin,i}$.

Each particle $i = 1, ..., N_p$ at position $\boldsymbol{x_i} \in \mathbb{R}^d$ and time $t \in \mathbb{R}^+$ then follows

$$\frac{\mathrm{d}^2\boldsymbol{x_i}}{\mathrm{d}t^2} = f\left(\left\|\frac{\mathrm{d}\boldsymbol{x_i}}{\mathrm{d}t}\right\|_2\right)\frac{\mathrm{d}\boldsymbol{x_i}}{\mathrm{d}t} - \frac{1}{N}\sum_{j=1,i\neq j}^{N}\nabla K\left(\left\|\boldsymbol{x_i}-\boldsymbol{x_j}\right\|_2\right), \tag{2.2}$$

for reference see, for example, (Gutleb, José A. Carrillo and S. Olver 2022b; Gutleb, José A. Carrillo and S. Olver 2022a). For now, we only consider the case without an external potential $V(\boldsymbol{x})$.

2.1.1 Attractive-Repulsive Potential

An example we will study is that of the attractive-repulsive interaction potential, where two power-law potentials compete with each other. For a given $\alpha, \beta \in \mathbb{R}\backslash\{0\}$, it is given by

$$K_{\alpha,\beta}(r) = \frac{r^\alpha}{\alpha} - \frac{r^\beta}{\beta}. \tag{2.3}$$

One can even consider the case when either α or β is 0 in order to arrive at a log-term (José A. Carrillo and Yanghong Huang 2017), using the convention that $\frac{x^0}{0} := \log(x)$[2]. If the repulsive term is stronger (so $\beta > \alpha$), there is no equilibrium distribution as particles simply continue repelling each other out to infinity. Attractive-repulsive potentials in general describe pairwise interactions with separate attractive and repulsive terms. In our case however, we will only refer to attractive-repulsive *powerlaw* potentials, specifically of the form in Equation (2.3).

The Lennard-Jones potential ($\alpha = -12, \beta = -6$), for example, is an **intermolecular** potential, so the relevant length-scale is between molecules. Therefore, the only relevant interaction is the electromagnetic force. Other forces, such as strong force which keeps protons in the nucleus together (a force much stronger than the electromagnetic one, but with much lower reach), need not be considered at this length-scale.

2.1.2 Morse Potential

Another frequently used pairwise interaction is the *Morse potential* $K_{C_a,l_a,C_r,l_r} : \mathbb{R}^+ \mapsto \mathbb{R}$ given by

$$K_{C_a,l_a,C_r,l_r}(r) := C_a\mathrm{e}^{-r/l_a} - C_r\mathrm{e}^{-r/l_r}, \tag{2.4}$$

[2]Consider the Laurent series expansion of $\frac{x^a}{a} = \frac{1}{a} + \log(x) + \frac{1}{2}a\log^2(x) + \mathcal{O}(a^2)$ in the limit as $a \to 0^+$. While this limit approaches ∞ coming from the right and $-\infty$ coming from the left due to the nature of the first term in the expansion, the only remaining term in it is $\log(x)$ which is thereby chosen as a convention.

with attractive parameters $C_a \in \mathbb{R}^+$ and $l_a \in \mathbb{R}^+$ (a 'natural length scale') and repulsive parameters $C_r, l_b \in \mathbb{R}^+$. Possible parameter ranges are given by $C_a l_a^{d-2} > 1, l_a < 1$ (D'Orsogna et al. 2006; Carillo, Y. Huang and Martin 2014).

To be done / included.

2.2 Continuous Limit

The evolution equation, in the continuous limit as $N_p \to \infty$, becomes

$$\frac{\partial \rho}{\partial t} = \nabla \cdot (\rho \nabla K * \rho) \ . \tag{2.5}$$

where $\rho : \mathbb{R} \mapsto \mathbb{R}$ is the particle density function.

Proof. **To be done / included.**

□

The solution ρ we are looking for within the scope of this dissertation is the *equilibrium measure* (cf. Definition 2.2.1) minimizing the total potential U.

Definition 2.2.1: Equilibrium Measure

For a given pairwise interaction potential $K : \mathbb{R} \mapsto \mathbb{R}$, the equilibrium measure $\rho : \mathbb{R} \mapsto \mathbb{R}$ is a measure chosen such that

$$U = \frac{1}{2} \iint K\left(\|\boldsymbol{x} - \boldsymbol{y}\|_2\right) \, \mathrm{d}\rho(\boldsymbol{x}) \, \mathrm{d}\rho(\boldsymbol{y}) \, ,$$

is minimised, where $\mathrm{d}\rho = \rho(\boldsymbol{x})\mathrm{d}\boldsymbol{x}$.

Also consider the total mass of the equilibrium distribution, given by

$$M = \int \mathrm{d}\rho = \int_{\mathrm{supp}(\rho)} \rho(\boldsymbol{x}) \, \mathrm{d}\boldsymbol{x} \, , \tag{2.6}$$

which, without loss of generality, we can choose as $M = 1$ to make $\rho(\boldsymbol{x})$ a *probability distribution*. Also note that, as the integrand of the above integrals, we sometimes refer to the interaction potential K as an integral kernel or simply *kernel*.

Definition 2.2.2: Function Space

To be defined, space that our equilibrium measures are in. Could be

$$L^2 := \{f : \mathbb{R} \mapsto \mathbb{R} | f \text{ square integrable?}\}$$

To be done / included.

2.2.1 The Problem

Finding the equilibrium measure ρ that minimises the total potential U given an interaction kernel K.

To be done / included.

2.3 Self-Propulsion

Makes it active matter. Self-propulsion and friction could be modelled as a quadratic of the form

$$f(v_i) = 1.6 - 0.5v_i^2\,,$$

where $v_i := \|\boldsymbol{v_i}\|_2 = \left\|\frac{\mathrm{d}\boldsymbol{x_i}}{\mathrm{d}t}\right\|_2$.

To be done / included.

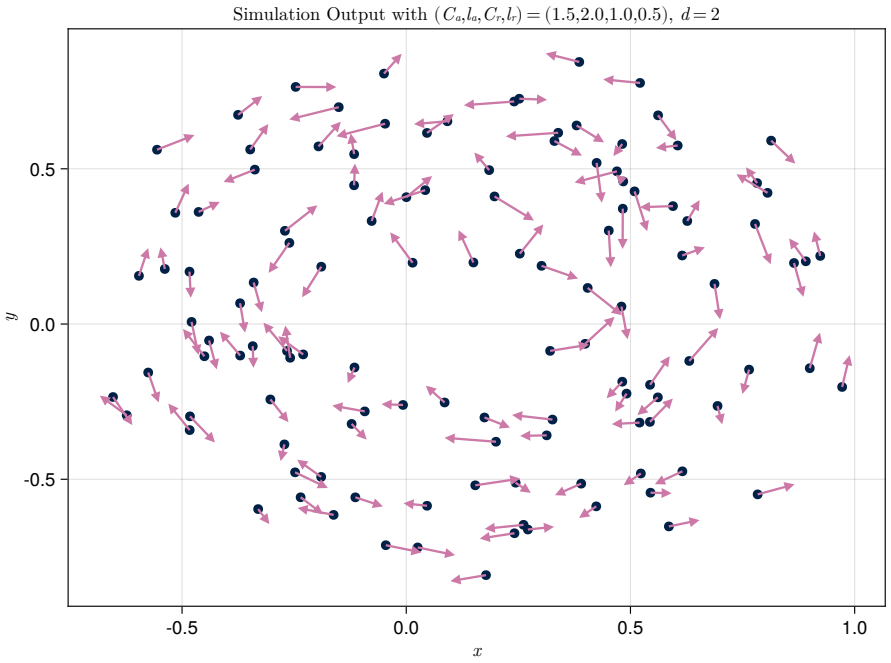

Figure 2.1: Position and velocity of $N_p = 120$ particles $d = 2$ dimensions as obtained through the molecular dynamics simulation introduced in Chapter 3. The interaction potential is a Morse potential with given parameters. Friction and self-propulsion terms are present as described in D'Orsogna et al. 2006, so using $f(v_i) = 1.6 - 0.5v_i^2$, this figure reproduces their results.

2.4 Kinetic Theory: The Vlasov Equation

A very common tool in Plasma physics.

$$\frac{\partial f}{\partial t} + \frac{\mathrm{d}\mathbf{r}}{\mathrm{d}t} \cdot \frac{\partial f}{\partial \mathbf{r}} + \frac{\mathrm{d}\mathbf{p}}{\mathrm{d}t} \cdot \frac{\partial f}{\partial \mathbf{p}} = 0,$$

This is the collisionless Boltzmann equation. Vlasov replaces the collision term with long-range interactions.

Theorem 2.4.1: Liouville's

Says that phase-space volume is conserved in situations of a pure particle-particle interaction.

$$\frac{d\rho}{dt} = \frac{\partial \rho}{\partial t} + \sum_{i=1}^{n} \left(\frac{\partial \rho}{\partial q_i} \dot{q}_i + \frac{\partial \rho}{\partial p_i} \dot{p}_i \right) = 0\,.$$

2.5 Vicsek Model

For the study of active matter (a number of individual agents).

To be done / included.

2.6 Swarming in Biological Settings

A 2010 paper by Cavagna et al. showed the surprising result that correlation between movement of individual starlings in bird flocks over Rome is scale-free. In contrast to the assumption that birds only mirror their neighbours' behaviour and swarming behaviour emerges as a result of that, this observation suggests that bird flocks exert collective behaviour beyond local interactions.

> The change in the behavioral state of one animal affects and is affected by that of all other animals in the group, no matter how large the group is (Cavagna et al. 2010).

This work was done by individually tracking each starling in the flock and using tracking algorithms to represent their 3 dimensional positions and velocities.

2.7 Analytical Solutions

José A. Carrillo and Yanghong Huang 2017 provides some analytic solutions to the problem. For example, when $\alpha = 2$ and $\beta \in [-1, 2]$, the equilibrium measure is given by

$$\rho(\boldsymbol{x}) = C_\beta \cdot R^d \cdot \left(R^2 - \boldsymbol{x}^2\right)^{\frac{1-\beta}{2}} , \tag{2.7}$$

where

$$C_\beta := \frac{1}{(\beta-1)\pi} \cos\left(\frac{(2-\beta)\pi}{2}\right) ,$$

$$R := \left(C_\beta \cdot B\left(\frac{1}{2}, \frac{3-\beta}{2}\right)\right)^{\frac{1}{\beta-2}} ,$$

with $B(\cdot,\cdot)$ the beta-function (cf. Definition 4.1.3).

Chapter 3

Particle Simulator

The aforementioned many-body systems generally exert very complex behaviour when viewed as a whole. This behaviour can be captured in mathematical terms but also from a simulation perspective. Particle simulations have been a subject of much attention in physics and scientific computing more generally. This class of simulations, in the context of intermolecular interactions, is often referred to as molecular dynamics.

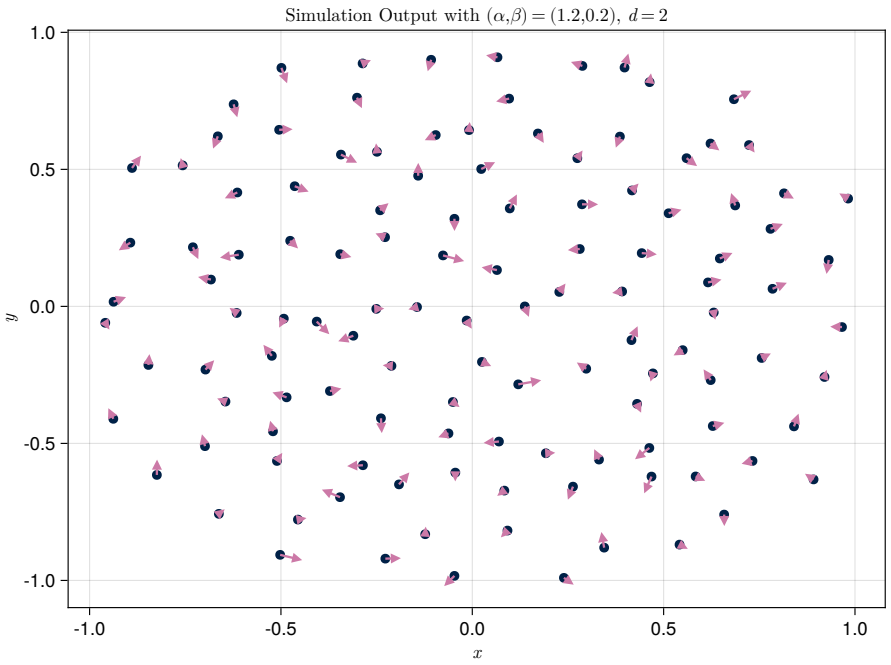

Figure 3.1: Position and velocity of particles in the simulation at a point in time. Every particle, each of equal mass m, interacts with every other particle through the interaction potential $U_{ij} = K\left(\|\boldsymbol{x_i} - \boldsymbol{x_j}\|_2\right)$ leading to $\mathcal{O}(N_p^2)$ interactions.

Because each particle interacts with every other particle, the number of interactions scales with $\mathcal{O}(N_p^2)$, which can play a prohibitive role in terms of the computation time when increasing the number of particles $N_p \gg 1$.

Within the scope of this thesis, in order to understand the elaborate behaviour of such particle systems and also to verify results from theory and the spectral method, we provide an implementation of a simulator starting from a numerical time integrator in $\mathbb{R}^d$. In addition to the *headless* simulation software, exporting state and results for treatment by the analysis component, a Graphical User Interface (GUI) is provided to enable live insight into and interaction with the model.

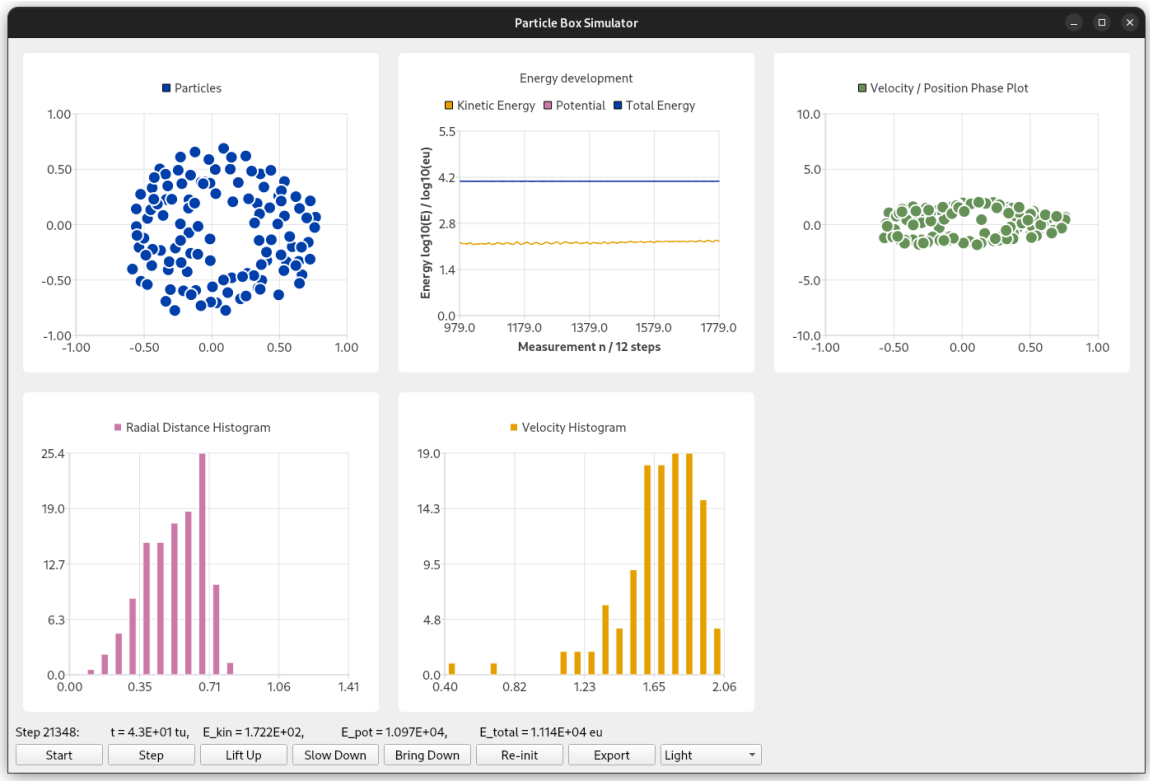

Figure 3.2: Screenshot of the GUI provided for the particle simulator. The top row shows the position of particles in their $[-1, 1]^d$ ($d = 2$ in this case) domain at a point t in time, the energy development over time and the current position/velocity phase space plot. Below, there are position and velocity histogram updated live along with the simulation.

3.1 Available Methods

- Simple Forward Integration
- Multistep Methods, which is an extension to the simple integration above.

- Fast Multipole Method
- Multigrid Methods

To be done / included.

3.1.1 Leapfrog Integration

Nice introduction here. Maybe compare with Advanced HMC?

To be done / included.

3.2 Phase Space

Each particle, at every point in time t, has a position and velocity value. In $d = 1$ dimension, one can visualise both of these quantities simultaneously in a phase space plot (cf. Section 3.2). For $d > 1$ dimension, it is possible to either only visualise the first components $\{\boldsymbol{x_i}\}_1$ and $\{\boldsymbol{v_i}\}_1$ or to visualise the norm of the position (distance from the center of mass) $r = \|\boldsymbol{x_i} - \boldsymbol{x}_{\text{center}}\|_2$ and velocity $\|\boldsymbol{v_i}\|_2$, where

$$\boldsymbol{x}_{\text{center}} := \frac{1}{N_p} \sum_{i=1}^{N_p} \boldsymbol{x_i} \, .$$

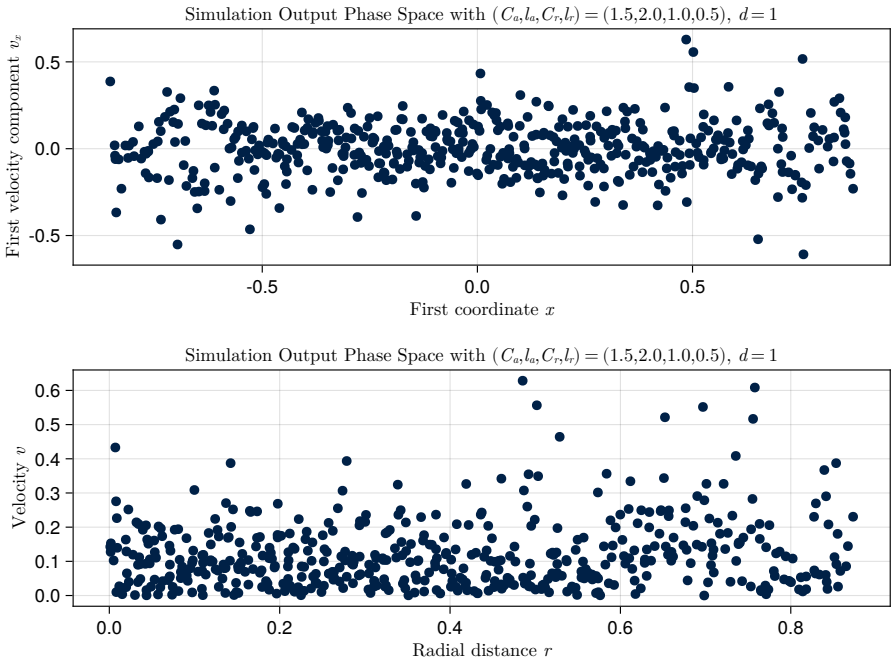

Figure 3.3: Position and velocity of $N_p = 500$ particles in a $d = 1$ simulation visualised as phase space plots using the two different visualisation mechanisms. In the top plot, one can observe natural rotation around the origin $(0, 0)$ as positive velocity corresponds to movement to the right and negative velocity to leftwards movement.

The behaviour of the phase space plot differs from potential to potential, most importantly one can observe multiple centers of rotation for the Morse potential in addition to the origin, whereas an attractive-repulsive potential builds up to an elliptical shape in the phase space plot.

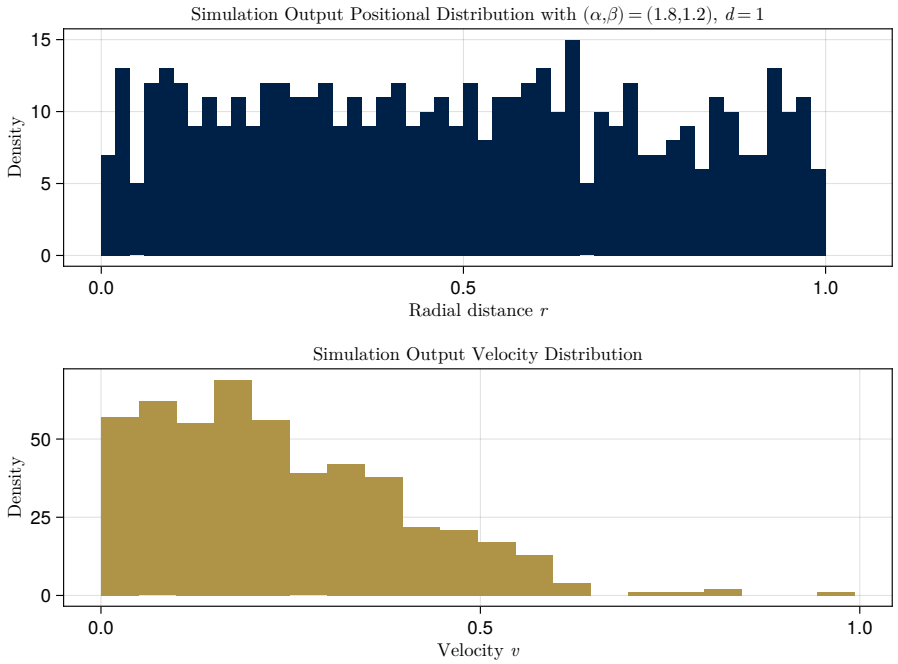

Figure 3.4: Radial Distance (r) and Velocity (v) Histograms as obtained through a long-running simulation of $N_p = 500$ particles interacting through an attractive-repulsive potential $K_{\alpha,\beta}(r)$. The spectral method introduced in Chapter 4 aims to solve for the particle density as a function of radial distance, hoping to predict the shape of the positional histogram.

In a physical setting with collision terms, the velocity distribution $f(v)$ would approach the shape of a Boltzmann distribution

$$f(v) = \left(\frac{m}{2\pi k_B T}\right)^{\frac{3}{2}} 4\pi v^2 \exp\left(-\frac{mv^2}{2k_B T}\right),$$

where k_B is the Boltzmann constant and T is temperature.

3.3 Runtime Analysis

To be done / included.

Chapter 4

Spectral Method

In this chapter we will construct a spectral method in the basis of Jacobi polynomials to explore the solution of equilibrium distributions $\rho(\boldsymbol{x})$. Starting from a many-body system and considering the continuous limit as $N_p \to \infty$, in Chapter 2 we have already established the governing equation of the particle density distribution $\rho(\boldsymbol{x})$ in such a system.

Can we put together a numerical method to solve for the equilibrium distribution (cf. Definition 2.2.1)? Let us consider the problem from the bottom up and start from the solution: The basic idea behind spectral methods is to assume a solution $\rho(\boldsymbol{x})$ of the form

$$\rho(\boldsymbol{x}) = \sum_{k=0}^{N-1} \rho_k \varphi_k(\boldsymbol{x}) \,, \quad \rho_k \in \mathbb{R}, \varphi_k : \mathbb{R}^d \mapsto \mathbb{R} \,, \quad k = 0, ..., N-1 \,,$$

with N coefficients $\boldsymbol{\rho} := (\rho_0, ..., \rho_{N-1})^T$ multiplying N basis functions φ_k.

4.1 Orthogonal Polynomials forming a Basis

The following section will introduce a few necessary objects and tools to understand the basis of functions we are working with to construct the spectral method, the basis of Jacobi polynomials.

We start with the Pochhammer symbol, another name for the *rising factorial*, an unusual notation for a function but standard in the context of the special functions that will be introduced on top of it.

Definition 4.1.1: Rising Factorial (Pochhammer Symbol)

The nth rising factorial of $x \in \mathbb{R}$ is given by

$$(x)_n := \prod_{k=0}^{n-1} (x+k) \ \in \mathbb{R}\,.$$

For example, $(3.141)_5 = 3.141 \cdot 4.141 \cdot 5.141 \cdot 6.141 \cdot 7.141$.

Remark 4.1.1: When the argument is a nonpositive integer, the rising factorial $(-m)_n = -m \cdot (-m+1) \cdot \ldots \cdot (-m+n-1)$ vanishes when $n \geq m+1$ for $n \in \mathbb{N}$ and $m \in \mathbb{N}_0$ as 0 is among the factors.

As a second prerequisite, we introduce the closely intertwined beta- and gamma-functions.

Definition 4.1.2: Gamma Function

Aligning with the factorial for integer arguments, $\Gamma : \mathbb{R}^+ \mapsto \mathbb{R}$ is given by

$$\Gamma(x) := \int_0^\infty t^{x-1} \mathrm{e}^{-t} \mathrm{d}t\,.$$

Remark 4.1.2: When $x \in \mathbb{R}, n \in \mathbb{N}_0$ such that $x, x+n \notin \mathbb{Z}_-$ are not negative integers, there is an important relation to the gamma function (Definition 4.1.2),

$$(x)_n = \frac{\Gamma(x+n)}{\Gamma(x)}\,.$$

Definition 4.1.3: Beta Function

$B : \mathbb{R}^+ \times \mathbb{R}^+ \mapsto \mathbb{R}$ is given by

$$B(x_1, x_2) := \int_0^1 t^{x_1-1}(1-t)^{x_2-1} \mathrm{d}t\,.$$

Note that following from this definition, there is a relationship with the gamma-function

$$B(x_1, x_2) = \frac{\Gamma(x_1)\Gamma(x_2)}{\Gamma(x_1+x_2)}\,.$$

In order to efficiently construct a spectral method, we need an orthogonal basis.

Definition 4.1.4: Orthogonal Polynomials

Are univariate polynomials

$$p : \mathbb{R} \mapsto \mathbb{R},\ p(x) = \sum_{k=0}^{N-1} c_k x^k \,.$$

that form an orthogonal basis under some inner product.

Theorem 4.1.1: Three-Term Recurrence Relationship

All orthogonal polynomials (cf. Definition 4.1.4) have (at least) a three-term recurrence relationship.

Proof. **To be done / included.**

□

For example, for the Chebyshev polynomials (cf. Definition 4.1.8) we have

$$T_{k+1}(x) = 2xT_k(x) - T_{k-1}(x)\,.$$

Using the Pochhammer symbol introduced in Definition 4.1.1, we can now define the generalised hypergeometric series ${}_pF_q$ (cf. Definition 4.1.5) and a special case of it, the Gaussian hypergeometric function (cf. Lemma 4.1.1).

Definition 4.1.5: Generalised Hypergeometric Series

The generalised hypergeometric series ${}_pF_q : \mathbb{R}^p \times \mathbb{R}^q \times \mathbb{C} \mapsto \mathbb{C}$ with $p, q \in \mathbb{N}$ is defined by

$${}_2F_1\left(\begin{matrix} a_1, \dots, a_p \\ b_1, \dots, b_q \end{matrix}; z\right) := \sum_{k=0}^{\infty} \frac{(a_1)_k \cdots (a_p)_k}{(b_1)_k \cdots (b_q)_k} \frac{z^k}{k!}\,,$$

where $(\cdot)_k$ denotes the rising factorial (cf. Definition 4.1.1).

Note that any permutation of the first ("top") arguments $a_1, ..., a_p$ leaves the function unchanged due to commutativity of multiplication on $\mathbb{C}$. The same holds for the second ("bottom") arguments $b_1, ..., b_q$.

Lemma 4.1.1: Gaussian Hypergeometric Function

The $p = 2$, $q = 1$ special case of the generalised hypergeometric series, commonly referred to as the Gaussian hypergeometric function, can also be evaluated by

$$ {}_2F_1\left(\begin{matrix} a_1, -n \\ b_1 \end{matrix}; z\right) = \sum_{k=0}^{n} (-1)^k \binom{n}{k} \frac{(a_1)_k}{(b_1)_k} z^k \,, $$

when the second argument $a_2 = -n$ is a nonpositive integer, so $n \in \mathbb{N}_0$.

Proof. Starting from the definition of the generalised hypergeometric series ${}_pF_q$ with $p = 2$ and $q = 1$ (Definition 4.1.5),

$$ {}_2F_1\left(\begin{matrix} a_1, -n \\ b_1 \end{matrix}; z\right) = \sum_{k=0}^{\infty} \frac{(a_1)_k (-n)_k}{(b_1)_k} \frac{z^k}{k!} = \sum_{k=0}^{n} \frac{(a_1)_k (-n)_k}{(b_1)_k} \frac{z^k}{k!} \,, $$

which can be terminated at $k = n$ due to Remark 4.1.1, we can express

$$ \frac{(-n)_k}{k!} = \binom{-n+k-1}{k} = (-1)^k \binom{1+n-k+k-1}{k} = (-1)^k \binom{n}{k} $$

using a well-known relation between the Pochhammer symbol and the binomial coefficient which immediately leads us to

$$ {}_2F_1\left(\begin{matrix} a_1, -n \\ b_1 \end{matrix}; z\right) = \sum_{k=0}^{n} \binom{n}{k} \frac{(a_1)_k}{(b_1)_k} (-z)^k \,, $$

concluding the proof. □

The Jacobi polynomials are then defined from ${}_2F_1$ as follows:

Definition 4.1.6: Jacobi Polynomials

Let $P^{(a,b)} : \mathbb{C} \mapsto \mathbb{C}$ with $a, b \in \mathbb{R}$ be given by

$$ P_n^{(a,b)}(x) := \frac{(a+1)_n}{n!} \, {}_2F_1\left(\begin{matrix} 1+a+b+n, -n \\ a+1 \end{matrix}; \frac{1-x}{2}\right) \,, $$

using the Gaussian hypergeometric function (Lemma 4.1.1) and the Pochhammer symbol (Definition 4.1.1).

Following from this definition,

$$ \begin{aligned} P_0^{(a,b)}(x) &= 1 \\ P_1^{(a,b)}(x) &= (a+1) + (a+b+2)\frac{x-1}{2} \end{aligned} $$

and so on. Also note that $\deg\left(P_k^{(a,b)}\right) = k$.

Lemma 4.1.2: Jacobi Polynomial Series

Definition 4.1.6 of $P_n^{(a,b)}$ is equivalent to

$$P_n^{(a,b)}(x) = \frac{\Gamma(a+n+1)}{n!\,\Gamma(a+b+n+1)} \sum_{k=0}^{n} \binom{n}{k} \frac{\Gamma(a+b+n+k+1)}{\Gamma(a+k+1)} \left(\frac{x-1}{2}\right)^k ,$$

where $\Gamma(x)$ is the gamma function (cf. Definition 4.1.2).

Proof. Inserting into Lemma 4.1.1, we have

$$\begin{aligned} P_n^{(a,b)}(x) &= \frac{(a+1)_n}{n!} \sum_{k=0}^{n} (-1)^k \binom{n}{k} \frac{(1+a+b+n)_k}{(a+1)_k} \left(\frac{1-x}{2}\right)^k \\ &= \frac{\Gamma(a+1+n)}{n!\cancel{\Gamma(a+1)}} \sum_{k=0}^{n} \binom{n}{k} \frac{\cancel{\Gamma(a+1)}\Gamma(1+a+b+n+k)}{\Gamma(a+1+k)\Gamma(1+a+b+n)} \left(\frac{x-1}{2}\right)^k \\ &= \frac{\Gamma(a+1+n)}{n!\Gamma(1+a+b+n)} \sum_{k=0}^{n} \binom{n}{k} \frac{\Gamma(1+a+b+n+k)}{\Gamma(a+1+k)} \left(\frac{x-1}{2}\right)^k \end{aligned}$$

using Remark 4.1.2. □

Special Cases: The Gegenbauer polynomials (cf. Definition 4.1.7) are a special case, namely when $a = b$. And Chebyshev Polynomials (cf. Definition 4.1.8) are a special case of them. In the special case when $a = b = 0$, they reduce to the Legendre polynomials $P_n(x) = P_n^{(0,0)}(x)$ F. Olver et al. 2018.

Dot-product notation. Note that in this manuscript we will use the dot-product notation

$$f(x) = \sum_{k=0}^{N-1} f_k P_k^{(a,b)}(x) \quad \Leftrightarrow \quad f(x) = \boldsymbol{f} \cdot \boldsymbol{P}^{(a,b)}(x) ,$$

to express that a function f is a linear combination of basis polynomials with coefficients $\boldsymbol{f} = (f_0, ..., f_{N-1})^T \in \mathbb{R}^N$. So $\boldsymbol{P}^{(a,b)}(x) \in \mathbb{R}^N$ is the vector of Jacobi polynomials $P_0^{(a,b)}(x)$, $P_1^{(a,b)}(x)$, ..., $P_{N-1}^{(a,b)}(x)$.

Lemma 4.1.3: Jacobi Polynomial Orthogonality

Jacobi polynomials $P_n^{(a,b)}(x)$ are orthogonal on $[-1, 1]$ with respect to the weight function

$$w^{(a,b)}(x) = (1-x)^a(1+x)^b\,,$$

so they satisfy

$$\int_{-1}^{1}(1-x)^a(1+x)^b P_n^{(a,b)} P_m^{(a,b)}\,\mathrm{d}x = \frac{2^{a+b+1}\Gamma(a+n+1)\Gamma(b+n+1)}{n!(a+b+2n+1)\Gamma(a+b+n+1)}\delta_{n,m}\,,$$

with $a, b > -1$, which uniquely determines $P_n^{(a,b)}(x)$.

Proof. See, for example, Arora and Bajpai 1995. □

- This basis yields a **sparse**, and in particular, **banded** operator.

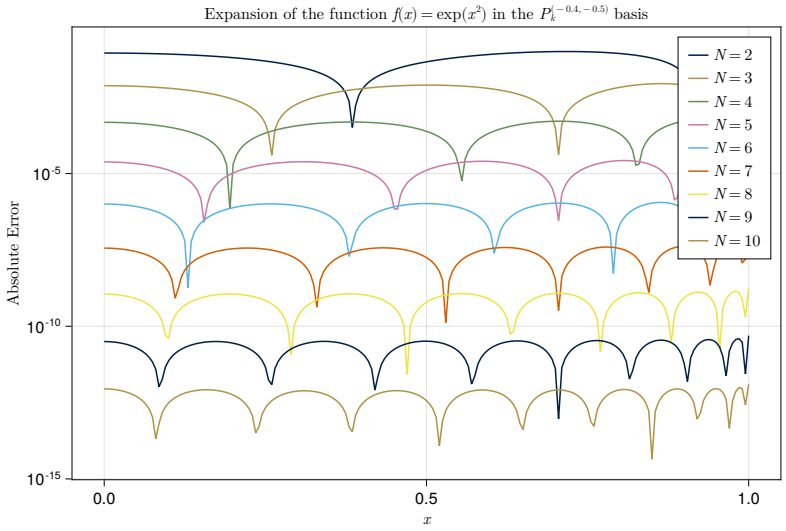

Figure 4.1: Convergence of the Jacobi polynomial expansion $f_N(x) = \sum_{k=0}^{N-1} P_k^{(a,b)}(x)$ of an example function $f(x) = \mathrm{e}^{x^2}$ with $a = -\frac{3}{4}$ and $b = -\frac{1}{2}$. Each added term improves the absolute error between the function and its expansion by a factor, so we have exponential convergence. The number of "arches" of each solution error function, occuring from the roots of $f(x) - f_N(x)$, approximately equals the order N.

Definition 4.1.7: Gegenbauer (Ultraspherical) Polynomials

$$C_n^{(\lambda)}(z) := \frac{(2\lambda)_n}{n!}\,{}_2F_1\left(-n, 2\lambda+n; \lambda+\frac{1}{2}; \frac{1-z}{2}\right) = \frac{(2\lambda)_n}{(\lambda+\frac{1}{2})_n} P_n^{(\lambda-1/2,\lambda-1/2)}(x)\,.$$

They satisfy a three-term recurrence relation (as all orthogonal polynomials do!)

$$\begin{aligned} C_0^{(\lambda)}(x) &= 1 \\ C_1^{(\lambda)}(x) &= 2\lambda x \\ (n+1)C_{n+1}^{(\lambda)}(x) &= 2(n+\lambda)xC_n^{(\lambda)}(x) - (n+2\lambda-1)C_{n-1}^{(\lambda)}(x). \end{aligned} \quad .$$

F. Olver et al. 2018, p. 18.9.1:

$$xC_n^{(\lambda)}(x) = \tfrac{(n+2\lambda-1)}{2(n+\lambda)}C_{n-1}^{(\lambda)}(x) + \tfrac{n+1}{2(n+\lambda)}C_{n+1}^{(\lambda)}(x). \tag{4.1}$$

From Wikipedia: In spectral methods for solving differential equations, if a function is expanded in the basis of Chebyshev polynomials and its derivative is represented in a Gegenbauer/ultraspherical basis, then the derivative operator becomes a diagonal matrix, leading to fast banded matrix methods for large problems (S. Olver and Townsend 2013).

Are a special case of the Jacobi Polynomials (cf. Definition 4.1.6) and form an Orthonormal Basis under the weight given by

$$w(x) = (1+x)^\alpha$$

Definition 4.1.8: Chebyshev Polynomials

Of the first kind:

$$T_k(x)$$

Of the second kind:

$$U_k(x)$$

Also have a Three-Term Recurrence Relationship, as given below Theorem 4.1.1.

In order to obtain a recurrence relationship between the coefficients later, we make use of the Jacobi matrix (cf. Definition 4.1.9).

Definition 4.1.9: Jacobi Matrix

The Jacobi operator is the matrix $X \in \mathbb{R}^{N\times N}$ satisfying

$$x \cdot P(x) = P(x) \cdot X^T .$$

Finally, now that we have established the basis functions, we can write down an ansatz $\rho : B_1(\mathbf{0}) \mapsto \mathbb{R}$ for the solution of the problem, of the form

$$\rho(\boldsymbol{x}) := \left(1 - \|\boldsymbol{x}\|_2^2\right)^{m-\frac{\alpha+d}{2}} \sum_{k=0}^{N-1} \rho_k P_k^{\left(m-\frac{\alpha+d}{2},\frac{d-2}{2}\right)}(2\|\boldsymbol{x}\|_2^2 - 1) . \tag{4.2}$$

with $P_k^{(a,b)}$ the Jacobi polynomials and $\{\rho_k\}_{k=0,\dots,N-1}$ the coefficients.

The spectral method can then be written as a linear system involving a matrix (operator).

Definition 4.1.10: Operator

Either the attractive or the repulsive operator can be sparse.
Obtained using Theorem 4.1.2.

Theorem 4.1.2: Integration Theorem that needs a name

On the d-dimensional unit ball B_1 the power law potential, with power $\alpha \in (-d, 2+2m-d)$, $m \in \mathbb{N}_0$ and $\beta > -d$, of the n-th weighted radial Jacobi polynomial

$$(1-|y|^2)^{m-\frac{\alpha+d}{2}} P_n^{\left(m-\frac{\alpha+d}{2},\frac{d-2}{2}\right)}(2|y|^2-1)$$

reduces to a Gaussian hypergeometric function as follows:

$$\begin{aligned}&\int_{B_1} |x-y|^\beta (1-|y|^2)^{m-\frac{\alpha+d}{2}} P_n^{\left(m-\frac{\alpha+d}{2},\frac{d-2}{2}\right)}(2|y|^2-1)\mathrm{d}y \\ &\quad = \frac{\pi^{d/2}\Gamma\left(1+\frac{\beta}{2}\right)\Gamma\left(\frac{\beta+d}{2}\right)\Gamma\left(m+n-\frac{\alpha+d}{2}+1\right)}{\Gamma\left(\frac{d}{2}\right)\Gamma(n+1)\Gamma\left(\frac{\beta}{2}-n+1\right)\Gamma\left(\frac{\beta-\alpha}{2}+m+n+1\right)} {}_2F_1\left(\begin{matrix} n-\frac{\beta}{2}, -m-n+\frac{\alpha-\beta}{2} \\ \frac{d}{2}\end{matrix}; |x|^2\right).\end{aligned}$$

Proof. Using

$$(-\Delta)^{-s}\left((R^2-\|\boldsymbol{y}\|_2^2)^q\right) = C_{q,s,d} R^{2q+2s} {}_2F_1\left(\begin{matrix} d/2-s, -q-s \\ d/2\end{matrix}; \frac{\|\boldsymbol{y}\|_2^2}{R^2}\right)$$

for $\|\boldsymbol{y}\|_2 \le R$ with $R = 1$ where $(-\delta)^{-s}$ denotes the inverse fractional Laplacian $\Delta := \nabla^2$ with power $s \in (0,1)$ and $q \in \mathbb{R}^+$ from Yanghong Huang 2014 based on the

Weber-Schafheitlin integral of two Bessel functions given in Milne-Thomson 1945.

$$C_{q,s,d} = \frac{2^{-2s}\Gamma(q+1)\Gamma(d/2-s)}{\Gamma(d/2)\Gamma(q+s+1)}$$

The Weber-Schafheitlin integrals are related to the fractional Laplacians of aforementioned functions because the Fourier transform of ${}_2F_1$ is a bessel function.

The fractional Laplacian $(-\delta)^{-s}$ is defined by Kwaśnicki 2017. □

Theorem 4.1.2 gives an explicit expression for the main integral $Q^\beta : L \mapsto L$, an operator from the Function Space L to the function space L, we are interested in:

$$\hat{Q}^\beta[\rho](x) = \int_{B_1} |x-y|^\beta (1-|y|^2)^{m-\frac{\alpha+d}{2}} P_n^{(m-\frac{\alpha+d}{2},\frac{d-2}{2})}(2|y|^2-1)\mathrm{d}y$$

which is used to construct the Spectral Method Operator Q^β (cf. Definition 4.1.10), acting on the coefficients $\boldsymbol{\rho}$.

Lemma 4.1.4: Mass

For a given solution $\rho : B_1(\mathbf{0}) \mapsto \mathbb{R}$, its *mass* $M \in \mathbb{R}$ is given by Equation (2.6). Provided the appropriate ansatz given in Equation (4.2), an expansion of weighted radial Jacobi polynomials with coefficients ρ_k, its *mass* is given by

$$M := \int_{\mathrm{supp}(\rho)} \rho(y)\,\mathrm{d}y = \frac{\pi^{d/2}\Gamma(a+1)}{\Gamma\left(a+d/2+1\right)}\rho_0\,,$$

so solely depending on the first coefficient ρ_0.

Proof (adapted from Gutleb, José A. Carrillo and S. Olver 2022a). To shorten notation, let $b := \frac{d-2}{2}$. The domain and radial symmetry of our problem suggests the use of hyperspherical coordinates:

$$\begin{aligned} M = \int_{B_1(\mathbf{0})} \rho(\boldsymbol{x})\,\mathrm{d}\boldsymbol{x} &= \sum_{k=0}^{N-1} \rho_k \int_{B_1(\mathbf{0})} \left(1-\|\boldsymbol{x}\|_2^2\right)^a P_k^{(a,b)}(2\|\boldsymbol{x}\|_2^2-1)\,\mathrm{d}\boldsymbol{x} \\ &= \sum_{k=0}^{N-1} \rho_k \int_{\partial B_1(\mathbf{0})} \mathrm{d}\Omega \int_{r=0}^1 (1-r^2)^a P_k^{(a,b)}(2r^2-1) r^{d-1}\,\mathrm{d}r \\ &= \Omega_d \sum_{k=0}^{N-1} \rho_k \int_{r=0}^1 (1-r^2)^a P_k^{(a,b)}(2r^2-1) r^{d-1}\,\mathrm{d}r\,, \end{aligned}$$

where $\Omega_d = 2\pi^{d/2}/\Gamma(d/2)$ is the surface area of the d-dimensional hypersphere (cf. Lemma 4.1.5) with radius $R=1$. Substituting $u := 2r^2-1$, therefore $r^2 = \frac{1+u}{2}$ and

$(1-r^2)^a = \left(\frac{1-u}{2}\right)^a = 2^{-a}(1-u)^a$ as well as $\mathrm{d}r = \frac{\mathrm{d}u}{4r}$,

$$\begin{aligned} M &= 2^{-a}\Omega_d \sum_{k=0}^{N-1} \rho_k \int_{u=-1}^{1} (1-u)^a P_k^{(a,b)}(u) r^{d-1} \frac{\mathrm{d}u}{4r} \\ &= 2^{-2}2^{-a}\Omega_d \sum_{k=0}^{N-1} \rho_k \int_{-1}^{1} (1-u)^a P_k^{(a,b)}(u) r^{d-2} \,\mathrm{d}u \,, \end{aligned}$$

we notice that $r^{d-2} = \left(\frac{1+u}{2}\right)^{\frac{d-2}{2}} = 2^{-b}(1+u)^b$ and so we have

$$\begin{aligned} M &= 2^{-2}2^{-a}2^{-b}\Omega_d \sum_{k=0}^{N-1} \rho_k \int_{-1}^{1} (1-u)^a (1+u)^b P_k^{(a,b)}(u) \,\mathrm{d}u \\ &= 2^{-(2+a+b)}\Omega_d \sum_{k=0}^{N-1} \rho_k \int_{-1}^{1} (1-u)^a (1+u)^b P_k^{(a,b)}(u) P_0^{(a,b)}(u) \,\mathrm{d}u \\ &= 2^{1-(2+a+b)} \frac{\pi^{d/2}}{\Gamma(d/2)} \sum_{k=0}^{N-1} \rho_k \frac{2^{a+b+1}\Gamma(a+1)\Gamma(b+1)}{0!(a+b+1)\Gamma(a+b+1)} \delta_{0,k} \\ &= \frac{\pi^{d/2}\Gamma(a+1)}{\Gamma\left(a+d/2+1\right)} \rho_0 \,, \end{aligned}$$

which relies on the classical orthogonality condition of the Jacobi polynomials given in Lemma 4.1.3 with the 0th polynomial $P_0(u) = 1$. □

Lemma 4.1.5: Surface area of the hypersphere

The surface area of the d-dimensional hypersphere $\partial B_R(\mathbf{0})$ is given by

$$\Omega_d(R) = \frac{\mathrm{d}}{\mathrm{d}R} V_d(R) = \frac{\mathrm{d}}{\mathrm{d}R}\left(\frac{2\pi^{d/2}}{d\Gamma(d/2)} R^d\right) = \frac{2\pi^{d/2}}{\Gamma(d/2)} R^{d-1} \,.$$

Proof. We find Ω_d by evaluation of the d-dimensional Gaussian integral

$$I_d := \int_{\mathbb{R}^d} \mathrm{e}^{-\|\boldsymbol{x}\|_2^2} \,\mathrm{d}\boldsymbol{x} = \int_{\mathbb{R}} \mathrm{d}x_1 \ldots \int_{\mathbb{R}} \mathrm{d}x_d \,\mathrm{e}^{-x_1^2-\ldots-x_d^2} = \left(\int_{\mathbb{R}} \mathrm{e}^{-x_1^2} \,\mathrm{d}x_1\right)^d = (I_1)^d \,,$$

using Fubini's theorem ($I_d < \infty$). Considering the case $d = 2$, we have

$$I_2 = \int_{\mathbb{R}^2} \mathrm{e}^{-\|\boldsymbol{x}\|_2^2} \,\mathrm{d}\boldsymbol{x} = \int_0^{2\pi} \mathrm{d}\theta \int_0^{\infty} r\mathrm{e}^{-r^2} \,\mathrm{d}r = -2\pi \int_0^{-\infty} \mathrm{e}^u \frac{\mathrm{d}u}{2} = \pi \int_{-\infty}^{0} \mathrm{e}^u \,\mathrm{d}u = \pi \,,$$

taking the classical approach of transitioning to polar coordinates r, θ (with Jacobi determinant r^{d-1} in the d-dimensional case) immediately leading us to $I_1 = \sqrt{\pi}$. Generalising this to higher dimensions d with hyperspherical coordinates,

$$I_d = \int_{\mathbb{R}^d} \mathrm{e}^{-\|\boldsymbol{x}\|_2^2} \,\mathrm{d}\boldsymbol{x} = \Omega_d \int_0^{\infty} r^{d-1}\mathrm{e}^{-r^2} \,\mathrm{d}r = \Omega_d \int_0^{\infty} s^{d/2-1}\mathrm{e}^{-s} \frac{\mathrm{d}s}{2} = \frac{\Omega_d}{2}\Gamma(d/2) \,,$$

where once again $r := \|\boldsymbol{x}\|_2$ and using a substitution $s := r^2$, we must find equality with the above result $I_d = \pi^{d/2}$,

$$I_d = \pi^{d/2} \overset{!}{=} \frac{1}{2}\Omega_d \Gamma(d/2) \quad \Leftrightarrow \quad \Omega_d = \frac{2\pi^{d/2}}{\Gamma(d/2)}\,.$$

Now integrating over the R-ball $B_R(\mathbf{0})$, we obtain $V_d(R) := |B_R(\mathbf{0})| = \Omega_d \int_0^R r^{d-1}\,\mathrm{d}r = \frac{\mathbb{R}^d \Omega_d}{d}$ and therefore $\Omega_d(R) = \frac{\mathrm{d}V_d(R)}{\mathrm{d}R} = \frac{2\pi^{d/2}}{\Gamma(d/2)} R^{d-1}$. □

4.2 Derivation of Operator

Based on the Three-Term Recurrence Relationship (cf. Theorem 4.1.1).

One can even determine an explicit relationship between the coefficients in the Jacobi expansion by considering the Jacobi Matrix (cf. Definition 4.1.9).

Considering the operator $\hat{Q}^\beta[\rho]$ as in Theorem 4.1.2, from the ansatz $\rho(\boldsymbol{x})$ (cf. Equation (4.2)) we have

$$\hat{Q}^\beta(x) = \sum_{k=0}^{N-1} \rho_k \int_{B_1(\mathbf{0})} \|\boldsymbol{x} - \boldsymbol{y}\|_2^\beta \left(1 - \|\boldsymbol{y}\|_2^2\right)^a P_k^{(a,b)}\left(2\|\boldsymbol{y}\|_2^2 - 1\right) \mathrm{d}\boldsymbol{y}\,. \tag{4.3}$$

We are now interested in a numerical representation of the operator $\hat{Q}^\beta$ acting on the function $\rho \in L^2$, so an equivalent (linear) operator $Q^\beta : \mathbb{R}^N \mapsto \mathbb{R}^N$ acting on the coefficients $\rho_k \in \mathbb{R}$, $k = 1, ..., N$. As every finite-dimensional linear operator must have a matrix representation, we are looking for a $Q^\beta \in \mathbb{R}^{N\times N}$ such that

$$\hat{Q}^\beta[\rho](\boldsymbol{x}) = \boldsymbol{P}_k^{(a,b)}\left(2\|\boldsymbol{x}\|_2^2 - 1\right) \cdot Q^\beta \boldsymbol{\rho}\,,$$

where $\boldsymbol{P}_k^{(a,b)}\left(2\|\boldsymbol{x}\|_2^2 - 1\right) \in \mathbb{R}^N$ is the vector of Jacobi polynomials $P_0^{(a,b)}(x)$, $P_1^{(a,b)}(x)$, ..., $P_{N-1}^{(a,b)}(x)$ evaluated at $2\|\boldsymbol{x}\|_2 - 1$ as introduced in and after Definition 4.1.6.

Therefore, starting from Equation (4.3), we obtain

$$\begin{aligned}\hat{Q}^\beta[\rho](\boldsymbol{x}) &= \sum_{k=0}^{N-1} \rho_k \hat{Q}^\beta[wP_k](\boldsymbol{x}) = \sum_{k=0}^{N-1} \rho_k \sum_{j=0}^{N-1} q_{kj} P_k^{(a,b)}\left(2\|\boldsymbol{x}\|_2^2 - 1\right) \\ &= \sum_{j=0}^{N-1}\sum_{k=0}^{N-1} \rho_k q_{kj} P_k^{(a,b)}\left(2\|\boldsymbol{x}\|_2^2 - 1\right)\,,\end{aligned}$$

which we will rewrite in matrix-form,

$$\hat{Q}^{\beta}[\rho](\boldsymbol{x}) = \boldsymbol{P}(\boldsymbol{x}) \cdot \begin{pmatrix} \sum_{k=0}^{N-1} \rho_k q_{k,1} \\ \vdots \\ \sum_{k=0}^{N-1} \rho_k q_{k,N} \end{pmatrix} = \boldsymbol{P}(\boldsymbol{x}) \cdot \underbrace{\begin{pmatrix} q_{11} & \cdots & q_{1N} \\ \vdots & \ddots & \vdots \\ q_{N1} & \cdots & q_{NN} \end{pmatrix}}_{=:Q^{\beta}} \begin{pmatrix} \rho_0 \\ \vdots \\ \rho_{N-1} \end{pmatrix}$$

$$= \boldsymbol{P}_k^{(a,b)}\left(2\left\|\boldsymbol{x}\right\|_2^2 - 1\right) \cdot Q^{\beta}\boldsymbol{\rho}$$

where we used $\boldsymbol{P}(\boldsymbol{x}) = \boldsymbol{P}_k^{(a,b)}\left(2\left\|\boldsymbol{x}\right\|_2^2 - 1\right)$ as a shorthand giving us the form of the operator matrix. Each value q_{kj} in it is therefore chosen to satisfy ...

To be done / included.

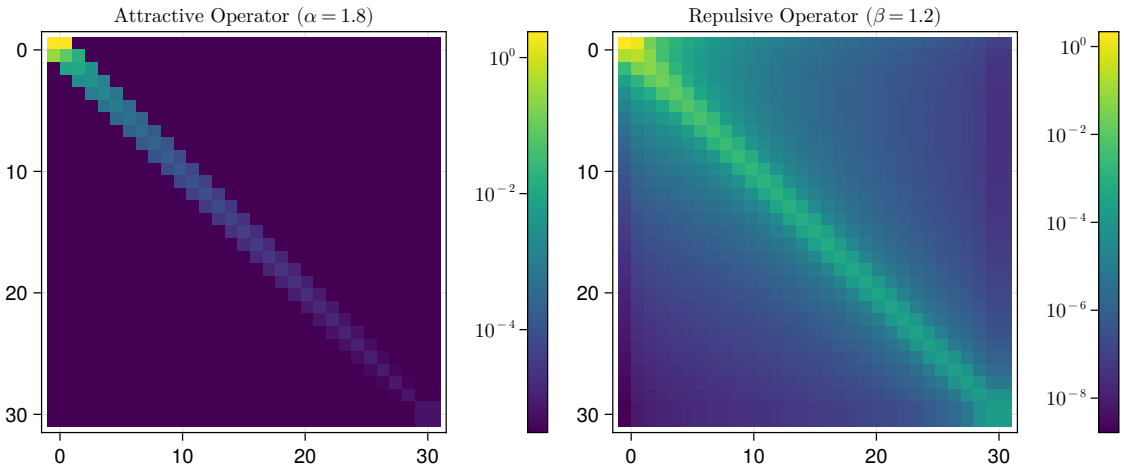

Figure 4.2: The attractive and repulsive operators (matrices) as given in Definition 4.1.10, the matrix values are shown in a $\log_{10}$ color scale. Due to the choice of basis, the attractive operator is exactly banded. The repulsive parameter is only approximately banded, which the spy plots effectively demonstrate.

The bandedness of the attractive operator is due to the three-term recurrence relationship of the Jacobi polynomial basis.

For the attractive-repulsive interaction potential, the full operator is given by

$$Q_{\alpha,\beta} := \frac{R^{\alpha}}{\alpha}Q^{\alpha} - \frac{R^{\beta}}{\beta}Q^{\beta} \tag{4.4}$$

for some interval radius $R \in \mathbb{R}^{+}$, usually chosen as the smallest possible R such that $\operatorname{supp}(\rho) \subseteq [-R, R]$.

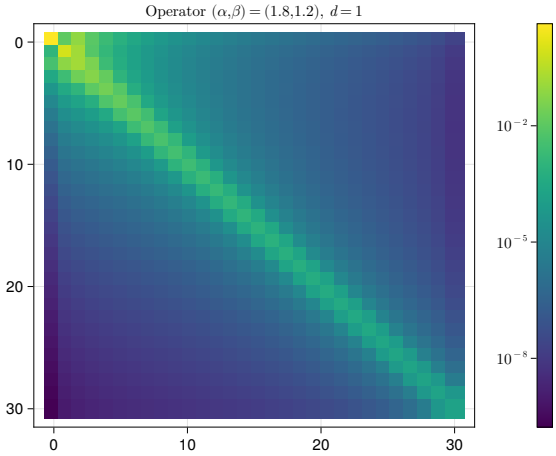

Figure 4.3: Spy plot of $Q_{\alpha,\beta}$, the combination of the attractive-repulsive operators. Inverting this operator and applying it to $(1, 0, ..., 0)^T \in \mathbb{R}^N$ will yield the unnormalised coefficients ρ_k of the solution expansion given in Equation (4.2).

4.3 Results

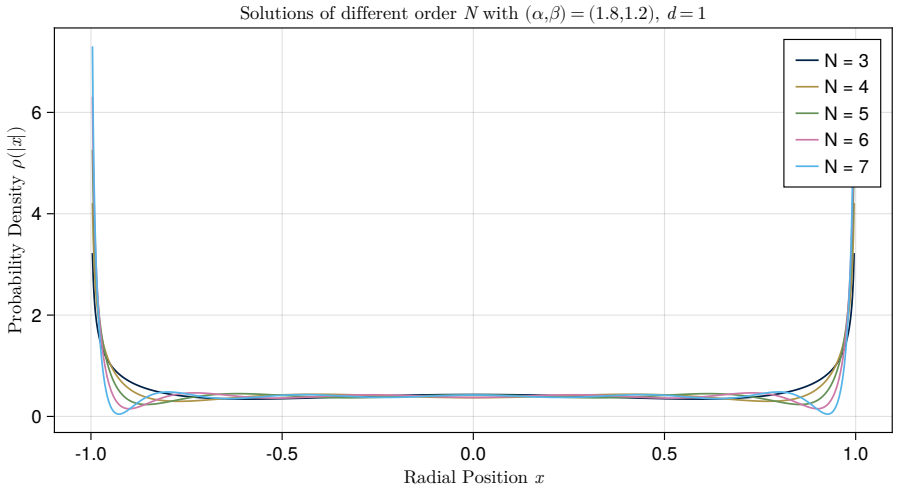

Figure 4.4: Particle density distribution function solutions ρ of increasing order N to the attractive-repulsive problem with interaction potential $K_{alpha,\beta}(r)$, $\alpha = 2.5$ and $\beta = 1.2$. Reflected along the y-axis for better visibility of the domain.

4.4 Outer Optimisation Routine

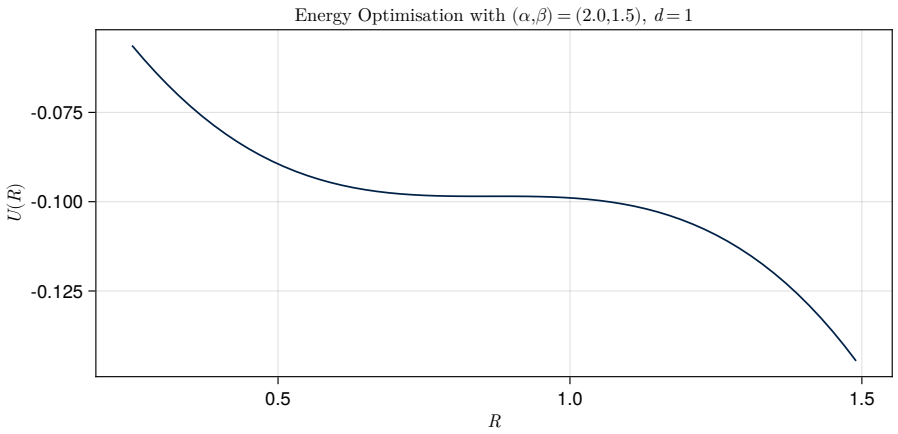

Figure 4.5: The total potential U as a function of the support radius R. This is the goal function minimised by the outer optimisation routine.

Note that using this setup, the operators themselves do not need to be recomputed upon a change in R (cf. Equation (4.4)). The provided implementation uses Least Recently Used (LRU) caching to automatically store operators for a given parameter set and order N.

4.5 Comparison with Analytic Solutions

As introduced in Section 2.7, there are some analytical solutions available which allow us to perform some further analysis of the numerical method in these special cases.

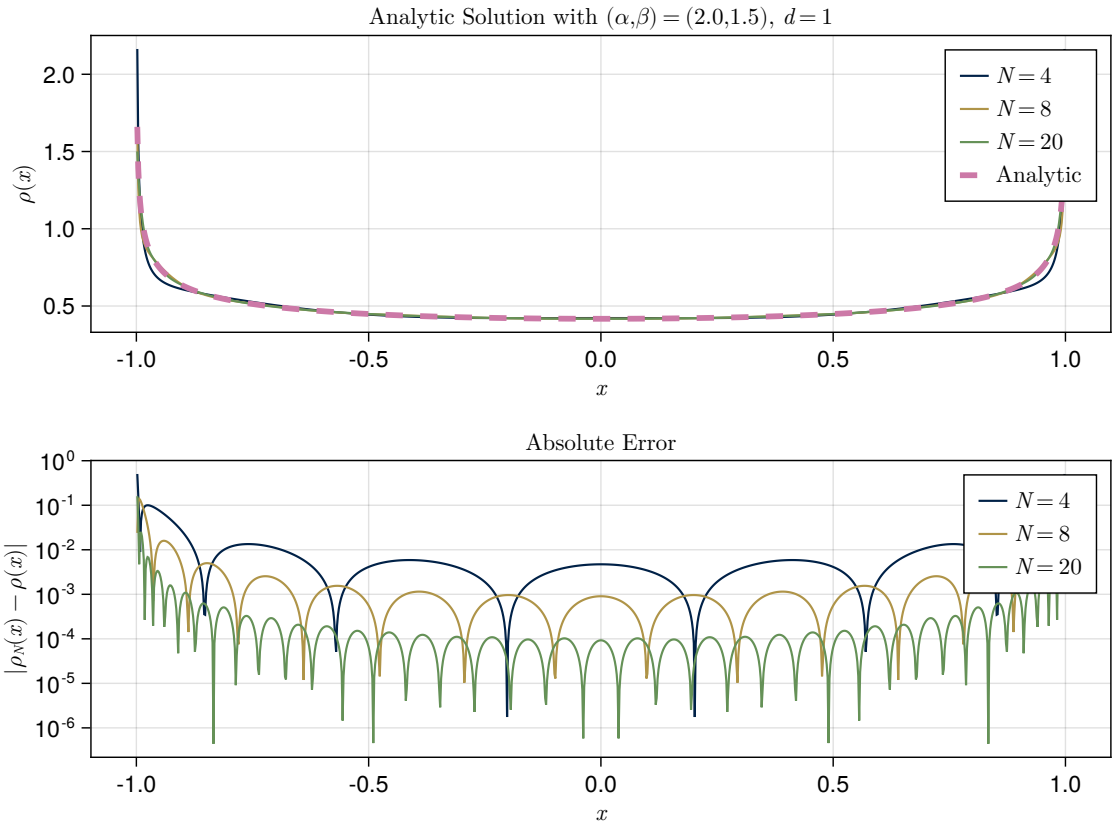

Figure 4.6: The analytic solution $\rho(x)$ given in Equation (2.7) compared to the (spectral method) solutions of different order N. The "arches" occur as a result of the roots of $\rho(x) - \rho_N(x)$, their number approximately equals the order N (a polynomial of degree N has N roots).

Definition 4.5.1: Spectral Convergence

Definition 3.6 (Convergence at spectral speed) An N -point approximation φ_N of a function f converges to f at spectral speed if $|\varphi_N - f|$ decays pointwise in $[-1, 1]$ faster than $O(N^{-p})$ for any $p = 1, 2, ...$ so $p \in \mathbb{N}$.

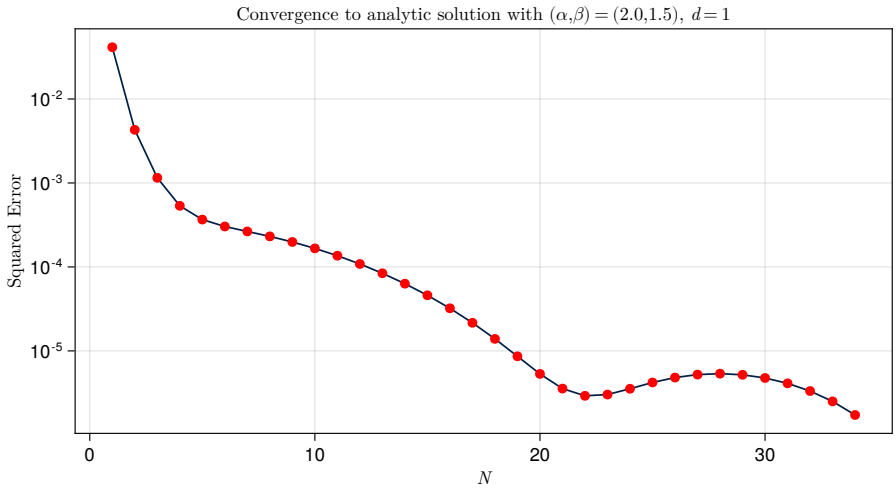

Figure 4.7: Convergence of the numerical solution to the known analytic solution (cf. Equation (2.7)) in a special case where it is known, squared error plotted as a function of the highest order in the expansion N.

4.6 Discussion

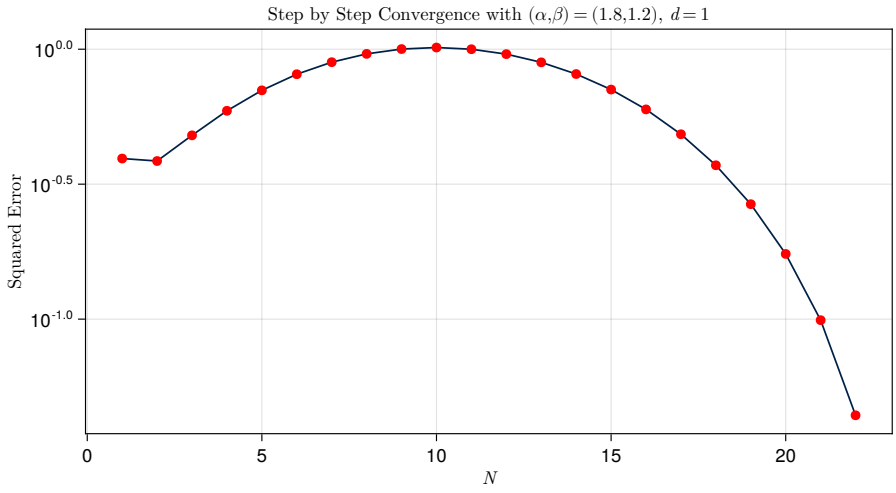

Figure 4.8: Step-by-step convergence of numerical solutions $\rho_N(x)$ as compared to $\rho_{24}(x)$, visualised using the squared error of the pointwise evaluation of both functions in 200 points.

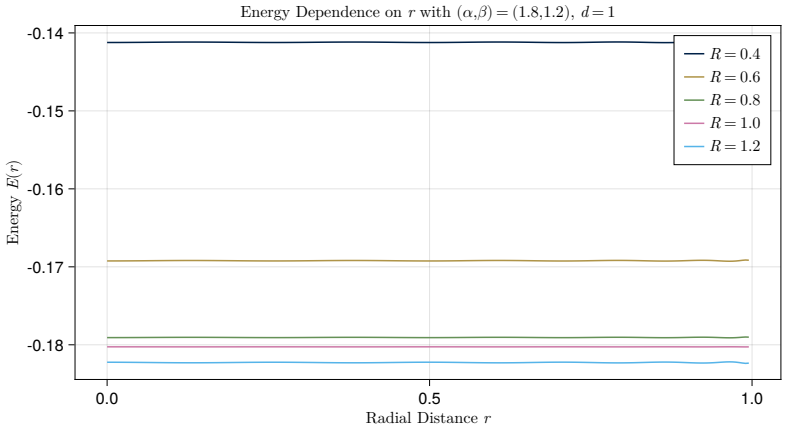

Figure 4.9: Plot of the spatial energy dependence on r, for different values of the domain support radius R. As one can see, they are constant and this figure is only present as visual proof to increase our confidence in the construction of the spectral method.

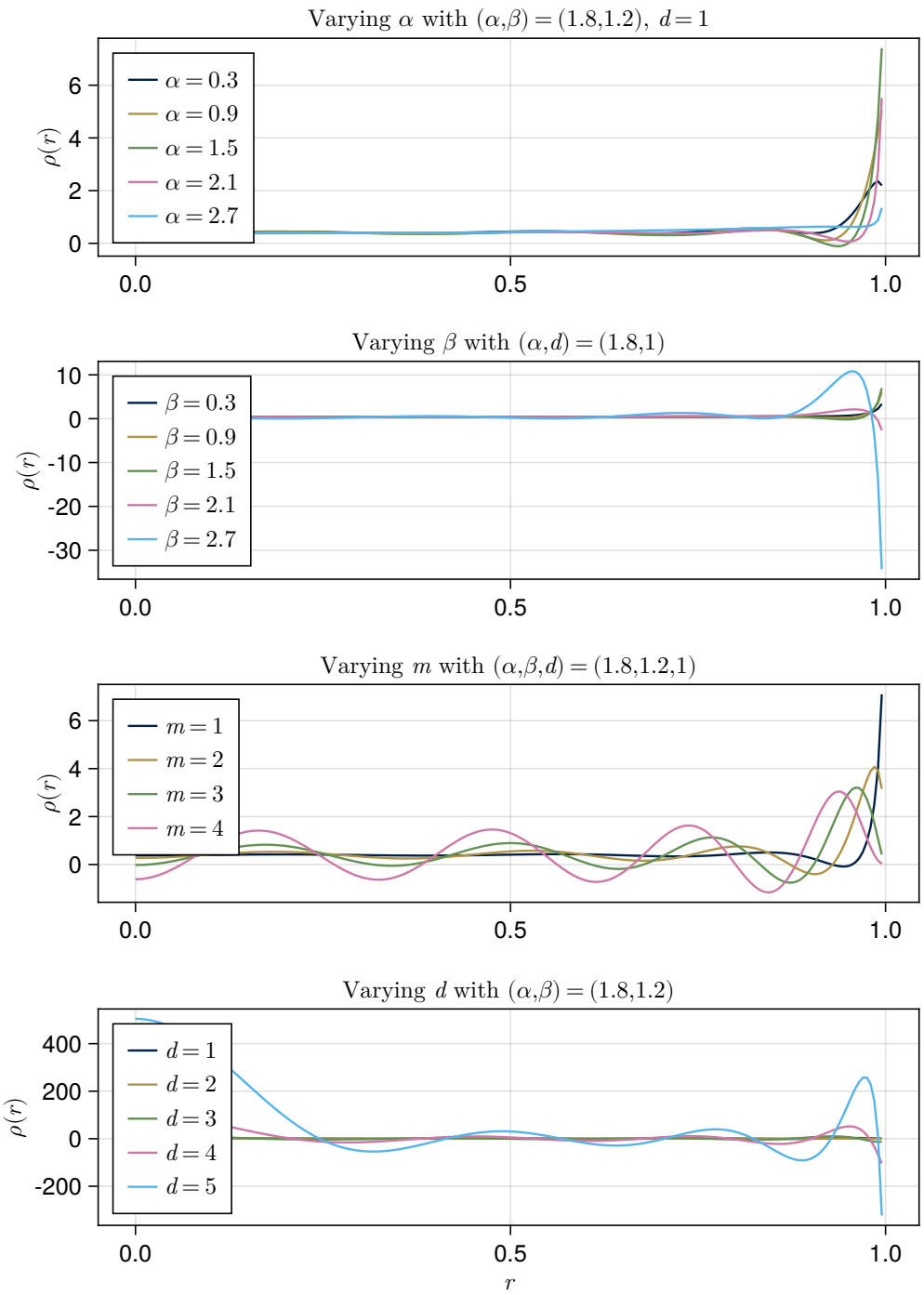

Figure 4.10: Varying different parameters in the solver to demonstrate their effect. See also, Chapter 5.

Chapter 5

General Kernel Spectral Method

Now that we know how to treat power-law potentials in the construction of a spectral method for the solution of equilibrium measures, can we consider more general kernels as well? The approach in this chapter will be to expand a general kernel K in a power-law basis and utilise the methodology introduced in the previous chapter to construct a general kernel spectral method.

More specifically, one choice of basis that could be made is the basis of monomials (so integer powers of the power-law kernel basis). Using standard methods from function approximation theory, we expand the general kernel $K : \mathbb{R}^+ \mapsto \mathbb{R}$ in the basis of G Jacobi polynomials (cf. Definition 4.1.6)

$$K(r) \approx \sum_{k=0}^{G-1} \tilde{g}_k P_k^{(a,b)} \left(2r^2 - 1\right) , \quad \tilde{g}_k \in \mathbb{R},\ k = 0, ..., G-1 ,$$

which we then reproject into the monomial basis to obtain the monomial coefficients $g_k \in \mathbb{R}$ such that

$$K_G(r) = \sum_{k=0}^{G-1} g_k r^k \approx K(r) , \quad g_k \in \mathbb{R},\ k = 0, ..., G-1 . \tag{5.1}$$

Does reprojection from Jacobi to monomials make sense / is it better for stability etc.? If so, explain reprojection using basis transformation matrix.

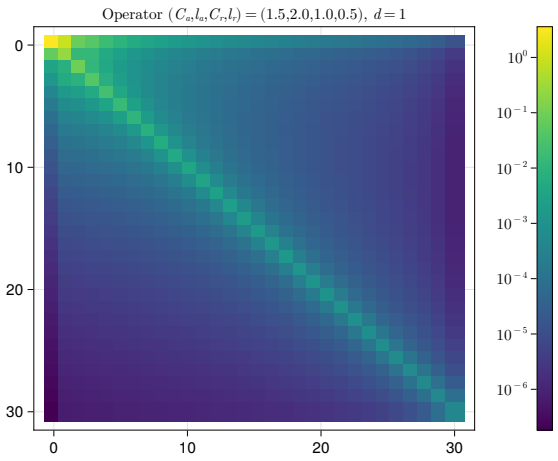

Figure 5.1: The full operator constructed from the $G = 8$th order monomial expansion K_G of the morse potential function $K_{C_a,l_a,C_r,l_r}(r)$ with parameters as given above.

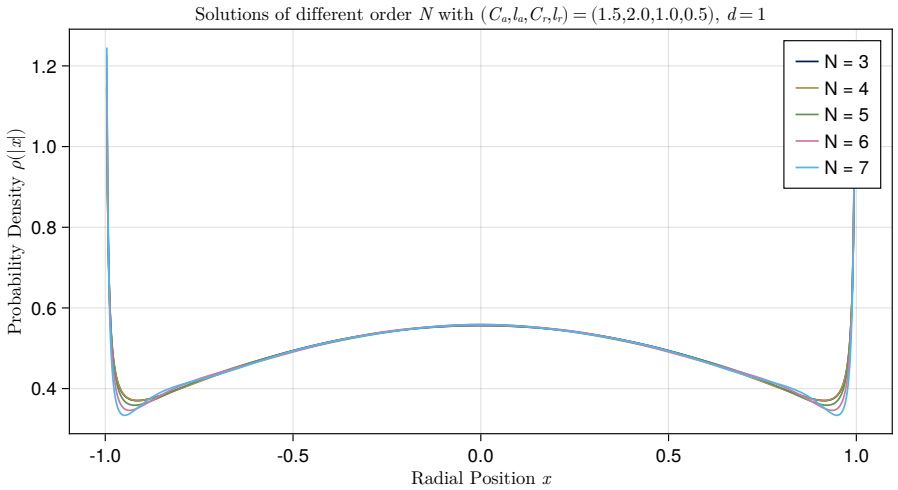

Figure 5.2: Solutions $\rho_N(x)$ of increasing order N in the general kernel setting with a monomial expansion of highest order $G = 8$ of the morse potential $K_{C_a,l_a,C_r,l_r}(r)$.

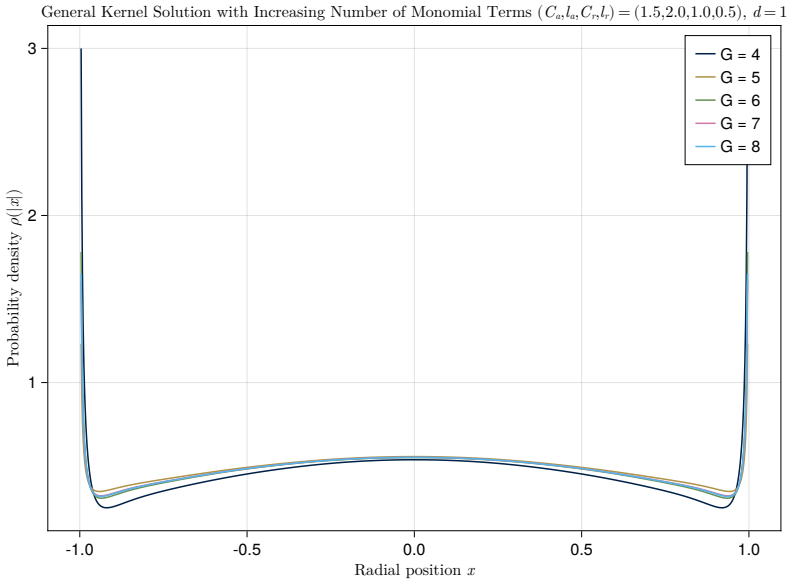

Figure 5.3: Solutions $\rho_8(x)$ for an increasing number of terms G in the monomial expansion of a general kernel K, in this case given by the morse potential $K_{C_a,l_a,C_r,l_r}(r)$. So each solution $\rho_8(x)$ is the sum of 8 Jacobi polynomials weighted by the solution coefficients.

As one can see, the solutions improve the better the approximation of the general kernel K becomes with growing order G of its monomial expansion. To make a better statement about this numerical behaviour, consider Chapter 5.

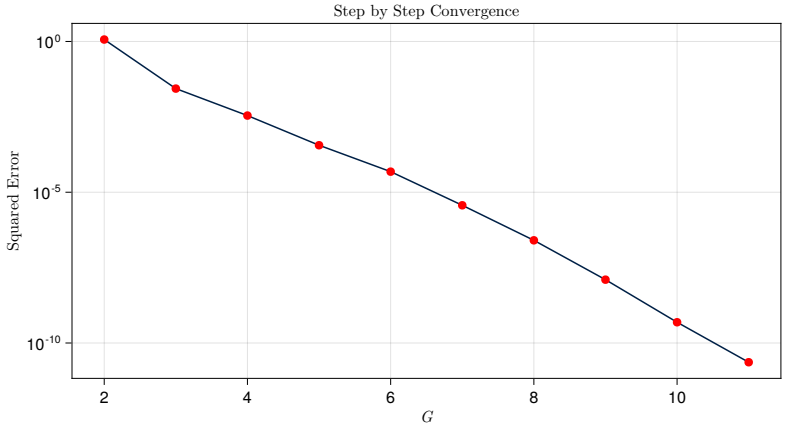

Figure 5.4: Convergence of numerical solutions $\rho_N(x)$ as compared to $\rho_{24}(x)$, visualised using the squared error of the pointwise evaluation of both functions in 200 points. The solver again uses $K(r) = K_{C_a,l_a,C_r,l_r}(r)$.

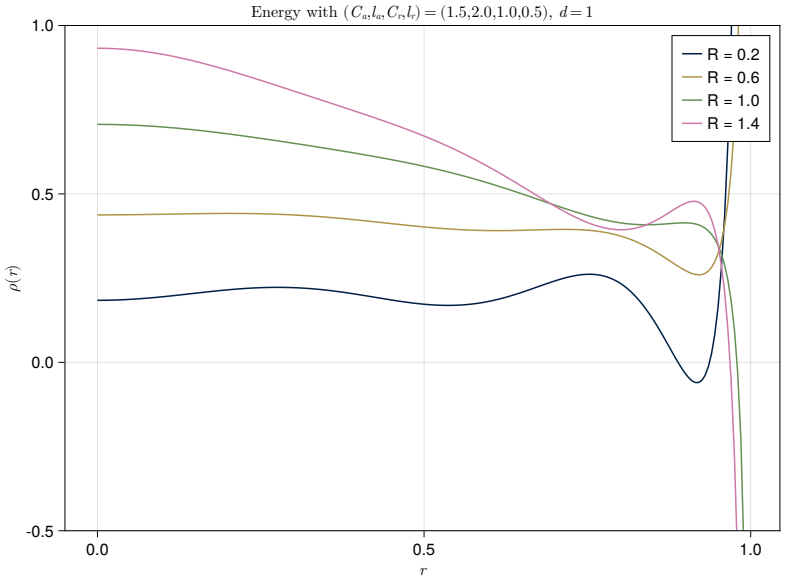

Figure 5.5: General kernel solutions ($N = 6$, $G = 8$) with varying R when using the Morse potential $K_{C_a,l_a,C_r,l_r}(r)$ with parameters as given above.

There is strong numerical evidence for ... (a "conjecture"). This is a current topic of discussion in the numerical analysis community.

Chapter 6

Implementation and Results

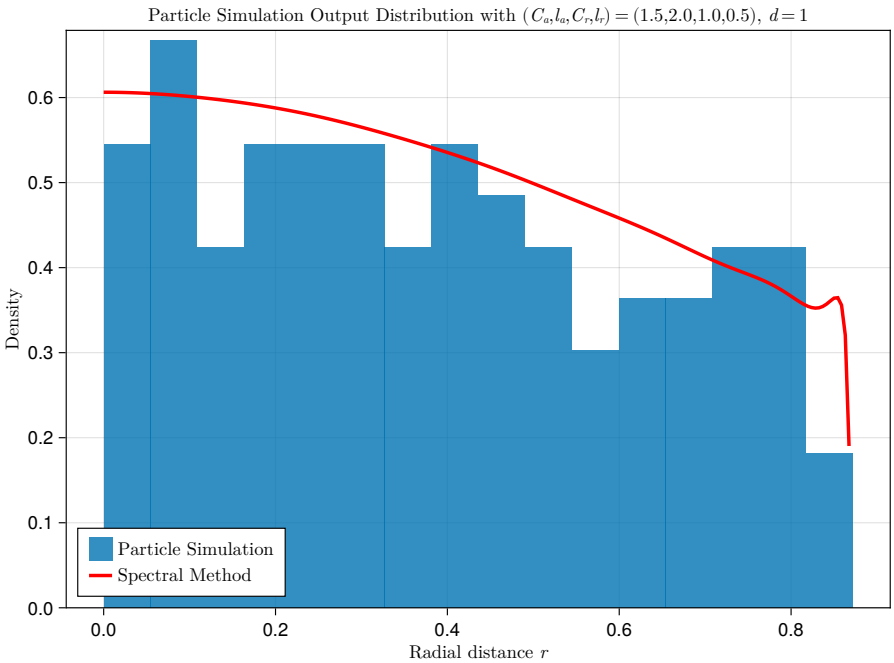

Figure 6.1: Comparison of the radial distance histogram from the simulation output with the $G = 8$ general kernel solvers' equilibrium measure $\rho_{12}(r)$ at R given by the simulator, so without using the outer optimisation routine. The interaction potential in this example is $K(r) = K_{C_a,l_a,C_r,l_r}(r)$ with parameters given above.

6.1 Further Discussion

6.1.1 Well-Conditionedness

A common flaw of spectral collocation methods, one could think of them as the highest-order limit of finite difference schemes, is their bad conditioning behaviour.

Ideally, we would like the condition number $\kappa(Q)$ to be independent of the order N to which we solve our problem. That means we want

$$\kappa(Q) := \frac{\sigma_{\max}(Q)}{\sigma_{\min}(Q)} = \frac{\|Q\|_2}{\|Q^{-1}\|_2} = \mathcal{O}(1)$$

and not $\mathcal{O}(N)$ or even higher orders.

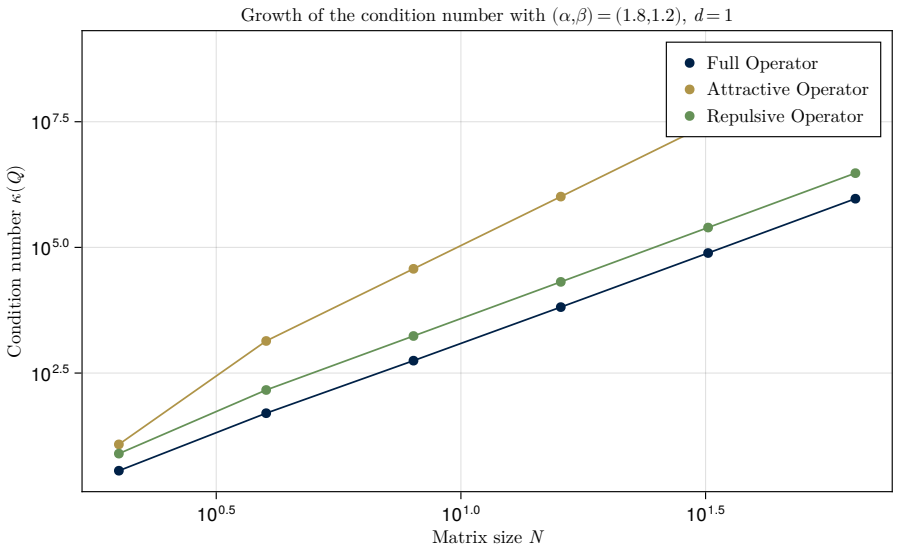

Figure 6.2: Growth of the 2-norm condition number $\kappa(Q)$ of the attractive-repulsive operator Q.

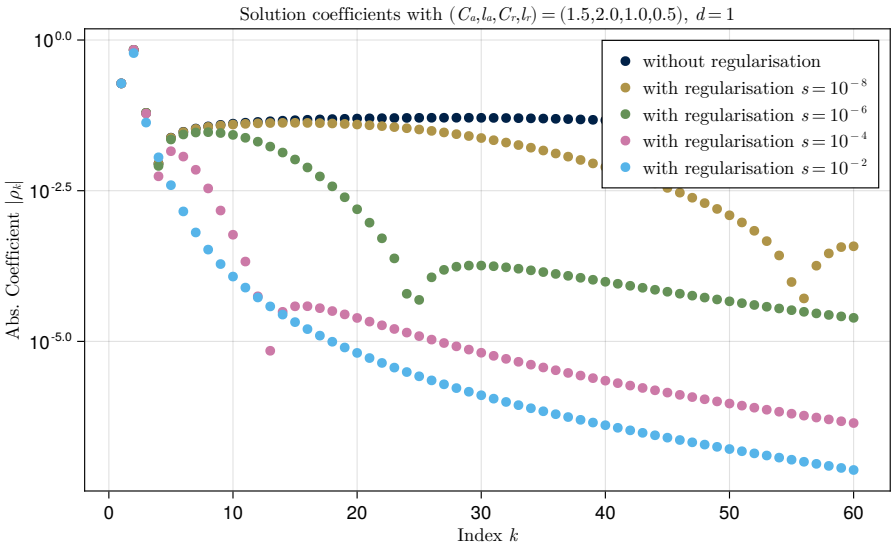

Figure 6.3: Absolute value of the solution coefficients ρ_k with and without Tikhonov regularisation.

6.2 Implementation Architecture

6.3 Runtime Analysis

The above benchmarks were accumulated on an Intel® i7-5600U CPU running at 2.6 GHz as the average over 3 individual runs with different test vectors, consistent across different parameter runs.

Chapter 7

Conclusion

Here we summarise the work that has been presented in this dissertation and discuss possible areas for future work.

7.1 Summary

Give a summary of what has been done. You might do this chapter by chapter but be sure to highlight all the important points.

In the present thesis, we explored the surprisingly complex behaviour of many body systems arising from simple pairwise particle-particle interactions and, in some cases, self-propulsion and friction terms. For certain types of interactions, these systems approach equilibrium distributions $\rho(\boldsymbol{x})$ which we aim to solve for using a spectral method, assuming their radial symmetry (a natural supposition in the absence of an external potential).

After introducing some theory in Chapter 2 and setting up a particle simulator to verify our findings in Chapter 3, we constructed a spectral method for power-law interaction potentials in Chapter 4 based on Jacobi polynomials. The resulting spectral method is a highly efficient direct method with excellent convergence properties and solvability due to the banded operators appearing in it. As an original extension, we introduced a numerical method for constructing the spectral solution for general kernels $K(r)$ in Chapter 5. Both methods reproduce analytical solutions to arbitrary precision and provide solutions for cases in which analytical solutions are unknown. We finally compared the numerical solution in the continuous situation with particle simulations in Chapter 6.

Next to the written part, the reader will find an implementation of the particle simulator written in C++ online (Waldert 2023), including a GUI, as well as the spectral method solver written in Julia.

7.2 Future Work

You don't actually have to list further work, but most people do this so it seems unusual not to. Just think what you would do next if you had more time on this project.

Other approaches, such as the one in Wu et al. 2015 show that ...

7.3 Conclusion

You might like to give a final conclusion so the reader is left remembering what you have done, rather than what you would do if there wasn't a submission deadline.

Acronyms, Definitions and Theorems

GUI Graphical User Interface 16
LRU Least Recently Used 33

Definitions

2.2.1 Equilibrium Measure . . . 11
2.2.2 Function Space . . . 12
4.1.1 Rising Factorial (Pochhammer Symbol) . . . 21
4.1.2 Gamma Function . . . 21
4.1.3 Beta Function . . . 21
4.1.4 Orthogonal Polynomials . . . 22
4.1.5 Generalised Hypergeometric Series . . . 22
4.1.6 Jacobi Polynomials . . . 23
4.1.7 Gegenbauer (Ultraspherical) Polynomials . . . 26
4.1.8 Chebyshev Polynomials . . . 26
4.1.9 Jacobi Matrix . . . 27
4.1.10 Operator . . . 27
4.5.1 Spectral Convergence . . . 34

Theorems

2.4.1 Liouville's . . . 13
4.1.1 Three-Term Recurrence Relationship . . . 22
4.1.2 Integration Theorem that needs a name . . . 27

Lemmata

4.1.1 Gaussian Hypergeometric Function 23
4.1.2 Jacobi Polynomial Series 24
4.1.3 Jacobi Polynomial Orthogonality 25
4.1.4 Mass 28
4.1.5 Surface area of the hypersphere 29

Remarks

4.1.1 21
4.1.2 21

Bibliography

Arora, Manmohan S. and S. D. Bajpai (Jan. 1995). 'A new proof of the orthogonality of Jacobi polynomials'. In: *Demonstratio Math.* 28.1, pp. 177–180. ISSN: 2391-4661. DOI: 10.1515/dema-1995-0122.

Bezanson, Jeff, Alan Edelman, Stefan Karpinski and Viral B Shah (2017). 'Julia: A fresh approach to numerical computing'. In: *SIAM review* 59.1, pp. 65–98. URL: https://doi.org/10.1137/141000671.

Carillo, J. A., Y. Huang and S. Martin (2014). 'Explicit flock solutions for Quasi-Morse potentials'. In: *European Journal of Applied Mathematics* 25.5, pp. 553–578. DOI: 10.1017/S0956792514000126.

Carrillo, José A. and Yanghong Huang (2017). 'Explicit equilibrium solutions for the aggregation equation with power-law potentials'. In: *Kinetic and Related Models* 10.1, pp. 171–192. ISSN: 1937-5093. DOI: 10.3934/krm.2017007.

Cavagna, Andrea, Alessio Cimarelli, Irene Giardina, Giorgio Parisi, Raffaele Santagati, Fabio Stefanini and Massimiliano Viale (June 2010). 'Scale-free correlations in starling flocks'. In: *Proc. Natl. Acad. Sci. U.S.A.* 107.26, pp. 11865–11870. DOI: 10.1073/pnas.1005766107.

D'Orsogna, M. R., Y. L. Chuang, A. L. Bertozzi and L. S. Chayes (Mar. 2006). 'Self-Propelled Particles with Soft-Core Interactions: Patterns, Stability, and Collapse'. In: *Phys. Rev. Lett.* 96.10, p. 104302. ISSN: 1079-7114. DOI: 10.1103/PhysRevLett.96.104302.

D'Orsogna, Maria R. (Dec. 2017). *Why do animals form swarms?* [Online; accessed 12. Aug. 2023]. URL: https://ed.ted.com/lessons/why-do-animals-form-swarms-maria-r-d-orsogna.

Danisch, Simon and Julius Krumbiegel (2021). 'Makie.jl: Flexible high-performance data visualization for Julia'. In: *Journal of Open Source Software* 6.65, p. 3349. DOI: 10.21105/joss.03349. URL: https://doi.org/10.21105/joss.03349.

Gutleb, Timon S., José A. Carrillo and Sheehan Olver (Dec. 2022a). 'Computation of Power Law Equilibrium Measures on Balls of Arbitrary Dimension'. In: *Constr. Approx.*, pp. 1–46. ISSN: 1432-0940. DOI: 10.1007/s00365-022-09606-0.

– (Sept. 2022b). 'Computing equilibrium measures with power law kernels'. In: *Math. Comput.* 91.337, pp. 2247–2281. ISSN: 0025-5718. DOI: 10.1090/mcom/3740.

Huang, Yanghong (Aug. 2014). 'Explicit Barenblatt profiles for fractional porous medium equations'. In: *Bull. London Math. Soc.* 46.4, pp. 857–869. ISSN: 0024-6093. DOI: 10.1112/blms/bdu045.

Kwaśnicki, Mateusz (Feb. 2017). 'Ten Equivalent Definitions of the Fractional Laplace Operator'. In: *FCAA* 20.1, pp. 7–51. ISSN: 1314-2224. DOI: 10.1515/fca-2017-0002.

Milne-Thomson, L. M. (Aug. 1945). *A Treatise on the Theory of Bessel Functions*. Vol. 156. 3955. Nature Publishing Group. DOI: 10.1038/156190a0.

Olver, F.W.J., A.B.O. Daalhuis, D.W. Lozier, B.I. Schneider, R.F. Boisvert, C.W. Clark, B.R. Miller and B. V. Saunders (eds.) (Dec. 2018). *NIST Digital Library of Mathematical Functions*. http://dlmf.nist.gov. (Visited on 11/11/2020).

Olver, Sheehan and Alex Townsend (Aug. 2013). 'A Fast and Well-Conditioned Spectral Method'. In: *SIAM Rev.* URL: https://epubs.siam.org/doi/10.1137/120865458.

Waldert, Peter (Aug. 2023). *Dissertation*. GitHub repository. URL: https://github.com/MrP01/Dissertation (visited on 30/08/2023).

Wu, Lei, Jun Zhang, Jason M. Reese and Yonghao Zhang (Oct. 2015). 'A fast spectral method for the Boltzmann equation for monatomic gas mixtures'. In: *J. Comput. Phys.* 298, pp. 602–621. ISSN: 0021-9991. DOI: 10.1016/j.jcp.2015.06.019.

List of Figures and Tables

List of Figures

2.1 Quiver plot of 120 particles in 2D interacting through the Morse potential 13

3.1 Quiver plot of 120 particles in 2D interacting through the attractive-repulsive potential 15
3.2 Graphical User Interface of the Simulator 16
3.3 Phase Space Plots 18
3.4 Radial Distance and Velocity Histograms of attractive-repulsive Simulation Output in 1D 19

4.1 Convergence of Jacobi basis expansion 25
4.2 Attractive and repulsive operators. 31
4.3 Combination of the attractive-repulsive operators 32
4.4 Solutions of increasing orders 32
4.5 Outer Optimisation Routine 33
4.6 Comparison with analytical solutions and error 34
4.7 Convergence to analytic solution 35
4.8 Step-by-step convergence of solutions compared to order 24 35
4.9 Spatial energy dependence on r 36
4.10 Varying parameters in the solver 37

5.1 Full Morse operator 39
5.2 General kernel solutions of increasing order 39
5.4 Step-by-step convergence of solutions when increasing the degree of the monomial 40
5.5 Solutions with varying R 41

6.1 Comparison of histogram and spectral method solution 42
6.2 Growth of the condition number 43
6.3 Absolute value of the coefficients with and without regularisation . . 44

A.1 Bump parameter solutions 53

List of Tables

Appendix A – Various Parameters

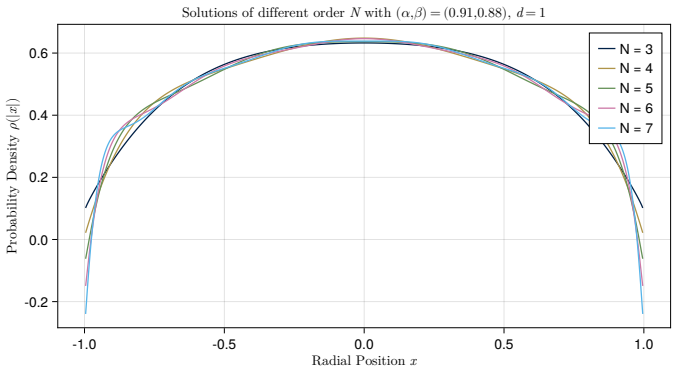

Figure A.1: Solutions with bump parameters.